1 **Title:** Scaling of G1 duration with population doubling time by a cyclin in *Saccharomyces*
2 *cerevisiae*
3

4 **Authors:** Heidi M. Blank, Michelle Callahan, Ioannis P.E. Pistikopoulos, Aggeliki O. Polymenis[1] and
5 Michael Polymenis
6

7 **Affiliations:** Department of Biochemistry and Biophysics, Texas A&M University, College Station, TX
8 77843, U.S.A.
9 [1]Present address: Department of Physics and Astronomy, University of California, Los
10 Angeles, CA 90095
11

12 **Correspondence:** blank@tamu.edu (H.M.B); polymenis@tamu.edu (M.P.)
13
14

15 **Running Title:** Scaling G1 with doubling time

ABSTRACT

A quantitative relation that defines the population doubling time (T_d) as a function of the time eukaryotic cells spend in specific cell cycle phases would be instrumental for estimating rates of cell proliferation and for evaluating introduced perturbations. Here, we show that in human cells the length of the G1 phase (T_{G1}) regressed on T_d with a slope of ≈0.75, while in the yeast *Saccharomyces cerevisiae* the slope was smaller, at ≈0.60. Levels of the yeast G1 cyclin Cln3p were positively associated with the growth rate over a broad range through translational control mediated by a short uORF in the *CLN3* transcript. Cln3p was also necessary for the scaling between T_{G1} and T_d. In contrast, yeast lacking the Whi5p transcriptional repressor maintained the scaling between T_{G1} and T_d. These data reveal fundamental scaling relations between the duration of eukaryotic cell cycle phases and rates of cell proliferation, point to the necessary role of Cln3p in these relations in yeast and provide a mechanistic basis linking Cln3p levels to growth rate and the scaling of G1 with doubling time.

Keywords: cell size / growth law / START / chemostat

35 **INTRODUCTION**

36 Recurring shapes and patterns in nature are sometimes described with mathematical relationships. As a
37 result, these natural processes can be predicted and understood better. Regarding patterns of
38 eukaryotic cell division, one could ask: How are the lengths of eukaryotic cell cycle phases related to
39 each other and to the total doubling time of the population? Can such relations be described
40 mathematically, in the form of a scaling formula? If so, what are the molecular mechanisms that govern
41 the scaling? A scaling relation that describes eukaryotic cell division would be an important advance. For
42 example, it could serve as a point of reference against which the effects of genetic or other
43 perturbations can be evaluated.

44 The 'textbook' view in the coordination of growth and division in the eukaryotic cell cycle (e.g., see
45 Fig. 10-26 in (MORGAN 2007)) is that expansion of the G1 phase of the eukaryotic cell cycle accounts for
46 most of the lengthening of the cell cycle in slower proliferating cells, in budding yeast (JOHNSTON *et al.*
47 1977; BRAUER *et al.* 2008) or humans (BASERGA 1985; FISHER 2016). However, there is no report in the
48 literature of a quantitative relation that defines the doubling time (T_d) as a function of the time yeast or
49 human cells spend in the G1 phase (T_{G1}). Here, we collected data for yeast and human cell populations
50 to derive, for the first time in the field, scaling relations between T_{G1} and T_d. These scaling relations also
51 allowed us to critically evaluate the role of cell cycle regulators in yeast cells growing at different rates.

52 Two key regulators of the length of the G1 phase in yeast are the Cln3p and Whi5p proteins. The G1
53 cyclin Cln3p promotes initiation of DNA replication (CROSS 1988; NASH *et al.* 1988). In contrast, the
54 transcriptional repressor Whi5p acts analogously to the retinoblastoma gene product in animals, to
55 inhibit the G1/S transition (COSTANZO *et al.* 2004; DE BRUIN *et al.* 2004; PALUMBO *et al.* 2016). It has been
56 reported that while synthesis of Cln3p parallels cell size, the synthesis of Whi5p is independent of cell
57 size (SCHMOLLER *et al.* 2015), arguing that dilution of Whi5p as cells get bigger in G1 governs the length of

58 the G1 phase (SCHMOLLER AND SKOTHEIM 2015; SCHMOLLER *et al.* 2015). We obtained the first
59 measurements of Cln3p and Whi5p levels as a function of growth rate in steady-state cultures. The
60 levels of Cln3p varied over a broad range as a function of growth rate, due to a uORF affecting
61 translation of *CLN3*. Our data also show that Whi5p is fully dispensable for the normal scaling relation
62 between T_d and T_{G1}, and provide instead the functional and molecular basis for the necessary role of
63 Cln3p in this process.

64 **MATERIALS AND METHODS**

65 **Strains.** Unless stated otherwise, *S. cerevisiae* wild-type, *cln3Δ* and *whi5Δ strains* were in the BY4741
66 background (NCBI Taxon 559292; *MAT*a*, his3Δ1, leu2Δ0, ura3Δ0, met15Δ0*) and they have been
67 described previously (SOMA *et al.* 2014). For protein surveillance, we constructed an otherwise wild type
68 strain that carried epitope-tagged *WHI5* and *CLN3* alleles at their endogenous chromosome locations.
69 First, a commercially available *WHI5-TAP::HIS3* strain (BY4741 otherwise; GE Healthcare) was
70 backcrossed three times into the W303 background (NCBI Taxon 580240; *MAT*α *leu2-3,112 trp1-1 can1-*
71 *100 ura3-1 ade2-1 his3-11,15*). Then, it was crossed with an otherwise wild-type strain carrying a *CLN3-*
72 *13MYC* allele (W303 background) described elsewhere (THORBURN *et al.* 2013), and kindly provided by
73 Dr. A. Amon (MIT and HHMI). The resulting diploid was sporulated and dissected, to obtain *MAT*a
74 haploid segregants carrying both the epitope-tagged *WHI5* and *CLN3* alleles (strains HB94/97; *MAT*a
75 *CLN3-13MYC::TRP*$^{+}$ *WHI5-TAP::HIS*$^{+}$ *leu2 ura3 met15*), which were used in the experiments shown in
76 Figure 4. We verified expression of Whi5p-TAP and Cln3p-$(Myc)_{13}$ in this strain (see Source Data,
77 Supplementary File 1), and their absence in *whi5Δ* or *cln3Δ* strains, respectively. We also generated a
78 derivative of this strain, which lacks the uORF in the 5'-leader of the *CLN3* mRNA. To this end, we used
79 plasmid A-315T-pMT10 we had described previously (POLYMENIS AND SCHMIDT 1997), as a template in a
80 PCR reaction with forward (5'-CAAGAACTACCATTCGACAGG-3') and reverse primers (5'-
81 CGTACAGAAAGCGTATCAAA-3') to generate a product that carries in the 5'-leader of *CLN3* the *URA3-*
82 marked A-315T mutation that inactivates the uORF. We then used this PCR product to transform strain
83 HB94 (*WHI5-TAP, CLN3-13MYC*). Genomic DNA of transformants was sequenced to verify the presence
84 of the A-315T mutation. Confirmed A-315T mutants were then backcrossed with wild type (W303) to
85 segregate away possible secondary mutations at other loci. The resulting heterozygote was sporulated
86 and dissected to isolate a *WHI5-TAP, A-315T-CLN3-13MYC* segregant (HB104), which was used in the
87 experiments shown in Figure 4.

88

89 **Measurements of G1 length.** The values we show in Tables S1 and S2 were obtained from studies
90 reporting on the doubling time (T_d) of asynchronous cell populations and the fraction of cells that are in
91 the G1 phase, reflecting the *relative* duration of the G1 phase. To estimate the *absolute* length of the G1
92 phase, T_{G1}, we multiplied the relative G1 length by T_d (Tables S1, S2). This simple equation is the
93 appropriate one to use with chemostat data when as many cells are removed as are being produced in
94 the culture (HOFFMAN 1949). Subtracting T_{G1} from T_d yields the duration of the rest of the cell cycle
95 phases (T_{nonG1}). For non-chemostat data, we recognize that other more elaborate equations could be
96 used, especially for the asymmetric patterns of division of budding yeast (HARTWELL AND UNGER 1977;
97 JOHNSTON *et al.* 1980). However, for simplicity and ease of comparison across systems, we uniformly
98 applied the simple equation mentioned above. Furthermore, inaccuracies in the absolute values of T_{G1}
99 may only affect the intercept of the linear relation between T_d and T_{G1}, but not the slope that describes
100 the fundamental scaling between T_d and T_{G1}, or any of our conclusions. Indeed, when we plotted in
101 exactly the same manner as in Figure 1 only the chemostat values in Table S1 (94 data points), the slope
102 of LnT_d vs. LnT_{G1} was 0.6107. For the remaining, non-chemostat values (55 data points), the slope of LnT_d
103 vs. LnT_{G1} was 0.6074.

104 Overall, the obtained variables represent population averages. They do not resolve
105 intergenerational differences in cell cycle progression of the same cells in successive cell cycles. It is also
106 assumed that cell death contributes negligibly to the doubling time of the population. This assumption is
107 reasonable in microbial culture systems because young cells vastly outnumber older ones approaching
108 senescence. However, it may be of concern in mammalian culture systems. Hence, our data with human
109 cells should be interpreted with caution, for at least two reasons: First, the fraction of growing cells in
110 the culture may be significantly lower than one. Second, although we are looking at trends that
111 seemingly hold across a multitude of different cells, the data were overwhelmingly derived from cancer

112 cell lines, which in many cases have altered cell cycles. In the context of this study, however, population
113 averages hold significant advantages: First, they are easily obtained; Second, they are ubiquitously used
114 and reported in the literature; Third, they allow straightforward comparisons between different
115 systems, for example between yeast and human cells (see Figure 1).

116 For yeast, the data we collected (Table S1) were from wild type strains from various backgrounds,
117 except in the few cases where they carried temperature-sensitive alleles, such as *cdc* mutations
118 (JAGADISH AND CARTER 1977), to estimate the length of the G1 phase upon transfer to the non-permissive
119 temperature. The methods used to calculate the fraction of G1 cells included: measurements of the DNA
120 content of the cells by flow cytometry (SLATER *et al.* 1977; JOHNSTON *et al.* 1980; GUO *et al.* 2004; BRAUER
121 *et al.* 2008; HENRY *et al.* 2010); budding (TYSON *et al.* 1979; RIVIN AND FANGMAN 1980); sensitivity to cell
122 cycle arrest before DNA replication by pheromone (HARTWELL AND UNGER 1977; JAGADISH AND CARTER
123 1977), or *cdc* (JAGADISH AND CARTER 1977) mutations. In this study, to obtain the fraction of G1 cells (e.g.,
124 see Figures 3, 4), we used DNA content measurements by flow cytometry, as described previously
125 (HOOSE *et al.* 2012; HOOSE *et al.* 2013). For human cells, earlier studies employed ^{3}H-thymidine pulses or
126 division waves after thymidine block (BASERGA 1985). The doubling times of the NCI-60 human cancer
127 cell lines we included in Table S2 are known (ROSS *et al.* 2000; SCHERF *et al.* 2000), but there was no
128 quantitative cell cycle data for most of the cell lines. However, images of DNA content profiles for the
129 NCI-60 panel, albeit with no quantification, have been published (GARNER AND EASTMAN 2011). We
130 requested and obtained high-resolution files of these images from Dr. Alan Eastman (Geisel School of
131 Medicine - Dartmouth College). From the entire DNA content histogram, to quantify the fraction of cells
132 in G1, we used imaging software to measure the area on the left side of the G1 peak (from peak to
133 valley) and multiplied this area by two, as has been described previously (JOHNSTON *et al.* 1980). This
134 approach avoids complications from heavy right side tails due to S phase cells and yields an acceptable
135 estimate of the relative G1 length as a fraction of total cell cycle time. We then combined these values

136 with all others available from human cells, cancerous and normal (SISKEN AND KINOSITA 1961; DEFENDI AND
137 MANSON 1963; LENNARTZ AND MAURER 1964; AOKI AND MOORE 1970; BASERGA 1985; KUMEI *et al.* 1989; BRONS
138 *et al.* 1992; LUCIANI *et al.* 2001; HAHN *et al.* 2009), to compile a dataset of 96 values for G1 length (T_{G1})
139 and doubling time (T_d) for human cells, shown in Table S2.

140

141 **Chemostat cultures.** The experiments were done using a New Brunswick BioFlo (BF-110) reactor with a
142 working volume of 880 mL, run at room temperature, as described earlier(HENRY *et al.* 2010). In each
143 experiment and at each dilution rate the reactor was sampled several times to measure protein levels by
144 immunoblots, the DNA content with flow cytometry, and the cell size and cell density of the culture
145 using a Beckman Z2 channelyzer (HENRY *et al.* 2010; HOOSE *et al.* 2012), as indicated. We measured the
146 cell density at every sampling, to ensure that we never reached 'wash-out' conditions at the high
147 dilution rates. In every experiment the cell density remained >1E+07 cells/ml, and did not vary more
148 than 3-fold between the lowest and highest dilution rates.

149

150 **Protein surveillance.** Protein were resolved onto 4-12% Tris-Glycine gels (Thermo Scientific, Cat#:
151 XP04125BOX). Cln3p-$(Myc)_{13}$ was detected with an anti-Myc antibody (Abcam, Cat #: ab13836). All other
152 procedures for TAP-tagged protein detection, extract preparation for immunoblots and their analysis
153 has been described elsewhere (BLANK *et al.* 2017).

154

155 **Statistical analysis.** All data were analyzed and displayed with R language packages. To build the linear
156 models we described using the values for the yeast (Tables S1) and human (Tables S2) datasets, we first
157 examined if the assumptions for building simple, linear parametric models were satisfied. The diagnostic

158 residual plots evaluating whether the errors were independent of each other, normally distributed
159 around a mean of zero and equal variance, are shown in Figure S2. In both the yeast and human
160 datasets, the existence of a few outlier points appeared to violate the necessary assumptions (Figure S2;
161 $p<0.05$ for assessment of the assumptions using the global test on 4 degrees-of-freedom, with the
162 'gvlma' function of the *gvlma* R language package (PENA AND SLATE 2006)). Hence, we opted for non-
163 parametric, robust linear regression models based on Siegel repeated medians (Table 1).

164 **RESULTS**

165 **Association between T_{G1} and T_d**

166 We compiled the available values for T_d and T_{G1} from the literature for budding yeast (Table S1) and
167 human (Table S2) cells (see Materials and Methods). To model T_{G1} against T_d, it is necessary to first
168 examine the distribution of T_{G1} values. We found that T_{G1} values were not normally distributed for yeast
169 (p = 4.434E-14, Shapiro-Wilk test, using the 'shapiro.test' function of the *stats* R package) or human cells
170 (p = 1.039E-07, Shapiro-Wilk test). Instead, T_{G1} values fit better a log-normal distribution. For example,
171 for yeast T_{G1} values, the Anderson-Darling statistic was the lowest for the log-normal distribution
172 (0.347), compared to other distributions (Weibull: 1.693; gamma: 1.521; exponential: 2.462), calculated
173 with the 'ad.test' function of the *nortest* R language package. As expected for log-normal distributions,
174 log-transformed values of T_{G1} were normally distributed for yeast (Figure S1A-D, p = 0.1871, Shapiro-
175 Wilk test) and human cells (Figure S1E-H, p = 0.3099, Shapiro-Wilk test). The apparent log-normal
176 distribution of T_{G1} values is consistent with a multiplicative process of many, positive, independent
177 random variables that determine G1 length (KOCH 1966). In cell proliferation, log-normality has been
178 proposed to reflect exponential patterns of growth in mass. Despite fluctuations in the growth rate
179 constant, the growth of the overwhelming majority of cellular components is influenced similarly,
180 leading to log-normality (KOCH AND SCHAECHTER 1962; KOCH 1966). In budding yeast and other cell types
181 there is evidence for exponential patterns of protein synthesis (ELLIOTT AND MCLAUGHLIN 1978; DI TALIA *et*
182 *al.* 2007) and increase in mass in the cell cycle (BRYAN *et al.* 2012; SON *et al.* 2012). Our data are
183 accommodated by such considerations and, for display purposes, we log-transformed the relevant
184 values (e.g., see Figure 1).

185 To test for association between T_{G1} and T_d we used the distribution-free Spearman's and Kendall's
186 tests for independence based on ranks. We opted for these non-parametric, distribution-free tests

187 because of the existence of outliers even in log-transformed T_{G1} values (e.g., see Figure S1). The high
188 values (> 0.75) of the rank correlation coefficients (τ for Kendall's and r for Spearman's; see Table 1)
189 show a strong positive association between T_{G1} and T_d, for both yeast (Figure 1A) and human (Figure 1C)
190 cells. Interestingly, however, the duration of the non-G1 phases (T_{nonG1}) of the cell cycle were also
191 positively correlated with T_d (Figures 1B, D; and Table 1) in both organisms, albeit less so in yeast
192 (τ=0.398; Figure 1B) than in human cells (τ=0.579; Figure 1D). Overall, these data document the tight
193 association between the duration of the G1 phase and population doubling time. Additionally, they
194 clearly show that growth requirements for cell division are also registered later in the cell cycle, in
195 agreement with observations from other groups (ANASTASIA *et al.* 2012; FERREZUELO *et al.* 2012; DOWLING
196 *et al.* 2014; SOIFER AND BARKAI 2014; CERULUS *et al.* 2016; MAYHEW *et al.* 2017).

197

198 **Lack of association between T_{G1}, or T_d, and cell size**

199 The size of yeast cells was not significantly associated with T_d (p-value= 0.171; Figure 2A) or T_{G1} (p-value=
200 0.2449; Figure 2B). The lack of association between cell size and T_d or T_{G1} may seem surprising in the
201 context of some earlier reports in yeast (TYSON *et al.* 1979), and the growth law in bacteria where an
202 exponential relation between cell size and doubling time (SCHAECHTER *et al.* 1958) accommodates
203 overlapping DNA replication cycles (SI *et al.* 2017). Based on those models, one would have expected a
204 negative association between size and growth rate, with cells getting smaller with larger T_d values. If
205 anything, in some nutrients yeast cells may become larger as they divide slower (note that some of the
206 largest cell sizes were recorded for long T_d values in Figure 2; see also Figure 4D, under leucine
207 limitation, where contrary to expectations cells appeared to increase in size as they divide slower
208 instead of getting smaller). Yet previous studies reported a negative association between growth rate
209 and cell size (TYSON *et al.* 1979). For example, we had also reported that cells proliferating slower in

210 media with poor carbon sources were smaller than cells proliferating faster in glucose-replete medium
211 (SOMA *et al.* 2014). However, all these examples were from batch cultures, where growth rate cannot be
212 adjusted independently of a specific nutrient. In contrast, in all examples from steady-state cultures,
213 when growth rate was adjusted independently of nutrient composition in yeast, there was no clear
214 pattern between T_d and cell size (GUO *et al.* 2004; BRAUER *et al.* 2008) (see also Figures 3, 4). Importantly,
215 in all these previous chemostat studies, cell size measurements were internally calibrated, and the lack
216 of any pattern of correlation between cell size and growth-rate cannot be attributed to experimental
217 variabilities of different studies incorporated in our meta-analysis of the literature in Table 1. Likewise,
218 from a genome-wide survey of single gene deletions (HOOSE *et al.* 2012), there was no pattern of
219 correlation between cell size and the relative duration of the G1 phase. Hence, although cell size can be
220 modulated by changes in nutrient composition in yeast, it is more likely that these are nutrient-specific
221 effects, not causally linked to growth rate changes. This interpretation is also consistent with models in
222 bacterial systems, which view cell size as a spandrel and the reported cell size effects of growth rate as
223 secondary to other causes (AMIR 2017).

224

225 **A scaling relation between T_{G1} and T_d**

226 To estimate a predictive and quantitative relation between T_{G1} and T_d we derived non-parametric,
227 robust linear regression models using the Siegel repeated median estimates (SIEGEL 1982), (Figure 1 and
228 Table 1; see also Materials and Methods). The intercepts of the linear T_{G1} vs. T_d plots reflect the
229 apparent minimum duration of the S+G2+M phases in yeast (1.4 h; Table 1) and human (7.6 h; Table 1)
230 cells. The slope of the regression of T_{G1} on T_d appeared to differ between the yeast and human datasets
231 (Figure 1 and Table 1). Applying the non-parametric Sen-Adichie test for parallelism, using the function
232 'sen.adichie' of the *NSM3* R package, confirmed that the difference in the slopes of the regression lines

233 of T_{G1} on T_d between yeast and human cells was statistically significant (V statistic = 7.324, p-value =
234 0.007). The particular slopes (≈0.6 for yeast and ≈0.75 for human cells) represent the exponents in the
235 linear relations of the corresponding log-transformed T_{G1} and T_d values. Such values are often
236 incorporated in scaling relations between the measured variables (CHAN AND MARSHALL 2010). For
237 example, a slope of ≈0.75 of the regression of T_d on T_{G1} brings to mind the famous Kleiber's law that an
238 animal's metabolic rate scales to the ¾ power of the animal's mass (CALDER 1981). The evidence we
239 presented above is not sufficient to make a case for any mechanistic connection with Kleiber's
240 parameters and the decision of human cells to initiate a new cell cycle. Instead, the quantitative
241 relations we identified linking T_{G1} with T_d are significant because they provide a framework to interpret
242 experimental perturbations in cell cycle progression and cell proliferation, as we describe next for yeast
243 cells.
244
245 **Loss of Cln3p, but not of Whi5p, alters the relation between T_{G1} and T_d**
246 To understand how the relation between the length of the G1 phase and doubling time is established in
247 budding yeast, we next examined the role of the Cln3p and Whi5p proteins, which regulate the G1/S
248 transition in this organism. It has been proposed that dilution of Whi5p as cells get bigger in G1 is the
249 key event controlling the timing of the G1/S transition (SCHMOLLER AND SKOTHEIM 2015; SCHMOLLER *et al.*
250 2015). Since in cells proliferating at different rates there is not a significant correlation with cell size
251 (Figure 2, Table S1), it is not clear how the inhibitor dilution model would apply to the conditions we
252 examine in this study. To test the role of Cln3p and Whi5p in the relation between T_{G1} and T_d, we
253 examined the cell cycle profile of *cln3Δ* or *whi5Δ* cells in continuous, steady-state chemostat cultures. To
254 our knowledge, the kinetics of cell cycle progression in cells lacking Cln3p or Whi5p have not been
255 examined previously in chemostat cultures. We measured T_{G1} in *cln3Δ* or *whi5Δ* cells from the DNA
256 content of the cultures under glucose (0.08% $^{w}/_{v}$) limitation and at different dilution rates (0.068 h^{-1} to

257 0.348 h^{-1}; corresponding to T_d values between 10 h and 2 h, respectively). As expected, cells lacking
258 Whi5p were very small (≈18 fL), and their size did not change significantly as a function of T_d (Figure 3C).
259 Furthermore, the intercept of the linear fit between the log-transformed T_d and T_{G1} values of *whi5Δ* cells
260 was higher than the intercept of the linear fit of these parameters in wild-type cells (1.17 vs. 0.92; see
261 Table 1), consistent with the shortened G1 phase of *whi5Δ* cells. Remarkably, however, the slope of the
262 linear relation between T_d and T_{G1} was similar to what we observed in wild-type cells (Figures 1A, 3A,
263 and Table 1; Sen-Adichie V statistic = 1.775, p-value = 0.183). Hence, although in absolute terms the G1
264 phase is shortened at all growth rates tested, *whi5Δ* cells nonetheless maintain the proportional
265 changes in T_{G1} and T_d upon nutrient limitation. Dilution of Whi5p in cells dividing in a given growth state
266 may account for the size dependency of the G1/S transition in that physiological state (SCHMOLLER *et al.*
267 2015). However, our data show that in different physiological states, and despite their shortened G1
268 phase and small size, *whi5Δ* cells remain fully responsive to different environments, displaying the
269 expected proportional changes between T_d and T_{G1}. In contrast, cells lacking Cln3p had an abnormal
270 behavior. T_{G1} did not even have a straightforward linear relation with T_d in cultures of *cln3Δ* cells. At
271 shorter division times, from T_d between 2 h and 6 h, the T_d and T_{G1} values of *cln3Δ* cultures were related
272 linearly (Figure 3B; slope = 0.7685), but this relation breaks down completely at low dilution rates, with a
273 T_d greater than ≈7-8 h (Figure 3B). At those long doubling times, the size of *cln3Δ* cells increased even
274 more than their already large cell size (Figures 3D). These data suggest that Cln3p, but not Whi5p, is
275 necessary for imposing the proper scaling relation between T_{G1} and T_d in wild type cells.
276

277 **Measurements of Cln3p and Whi5p steady-state levels at different growth rates**

278 Given the necessary role of Cln3p in establishing the physiological relation between T_d and T_{G1} (Figure 3),
279 we sought to measure the levels of Cln3p and Whi5p as a function of growth rate. There are no reports
280 of the steady-state levels of Cln3p or Whi5p in cell populations proliferating at different rates in

281 chemostats. To measure Whi5p and Cln3p levels from the same cells, we generated a strain that carries
282 *WHI5-TAP* and *CLN3-13MYC* alleles, providing the only source of these gene products in the cells,
283 expressed from their endogenous chromosomal locations (Figure 4A, see Materials and Methods). The
284 expressed proteins were epitope-tagged, but otherwise un-mutated, wild type Whi5p-TAP and Cln3p-
285 $(Myc)_{13}$. These cells were then cultured in continuous, steady-state chemostat cultures under glucose
286 (0.08% $^{w}/_{v}$) or leucine (0.0015% $^{w}/_{v}$) limitation. Although the *CLN3-13MYC* allele provides the means for
287 reliable detection of otherwise wild type Cln3p, it is known to be hypermorphic, stabilizing the Cln3p
288 protein somewhat and shortening the G1 phase of the cell cycle (THORBURN *et al.* 2013). Indeed, the
289 intercept of the linear fit between the log-transformed T_d and T_{G1} values of this strain (HB94; *WHI5-TAP*,
290 *CLN3-13MYC*) was higher than the intercept of the linear fit of these parameters in wild-type cells (0.97
291 vs. 0.92; see Table 1), consistent with a shortened G1 phase. Furthermore, the slope of the linear
292 relation between the log-transformed values of T_d and T_{G1} was increased (0.68 vs. 0.6; see Table 1),
293 arguing that even moderate stabilization of the Cln3p protein alters the relation between T_d and T_{G1}.
294 Nonetheless, these cells still displayed a strong, linear, positive association between T_d and T_{G1} (τ=0.77;
295 r=0.92; see Table 1). Hence, we proceeded to quantify the levels of both Whi5p-TAP and Cln3p-$(Myc)_{13}$,
296 from separate chemostat experiments under glucose or leucine limitation, each run at ≥5 different
297 dilution rates (Figure 4; see Materials and Methods). Surprisingly, the levels of Whi5p-TAP were reduced
298 in slower proliferating cells (Figure 4A, B). Previously, it was reported that Whi5p abundance increases
299 ≈3-fold in cells growing in poorer carbon sources (LIU *et al.* 2015). There are several variables that were
300 different between that study and ours, which could account for the disagreement in the findings: First,
301 different epitope-tagged alleles were used (*WHI5-tdTomato* vs. *WHI5-TAP*). Second, different detection
302 methods were applied (fluorescence live cell imaging vs. immunoblots). Third, and most significantly,
303 nutrient-specific effects could not be separated from growth rate-specific ones in (LIU *et al.* 2015).

304 We observed a much more significant and disproportionate reduction of Cln3p-$(Myc)_{13}$ levels in
305 slower-proliferating cells (Figure 4A, B). Normalized against the total cellular protein content, the fastest
306 proliferating populations had >10-fold higher levels of Cln3p-$(Myc)_{13}$ compared to the slowest
307 proliferating cells (Figure 4A, B). Furthermore, because these estimates rely on the hypermorphic *CLN3-*
308 *13MYC* allele that produces a more stabilized Cln3p protein (THORBURN *et al.* 2013), the dynamic range of
309 Cln3p levels as a function of growth rate is likely even greater.
310
311 **A uORF in *CLN3* adjusts the levels of Cln3p at different growth rates**
312 What is the mechanism that underpins the growth rate-dependent control of Cln3p abundance? We had
313 predicted that a uORF in *CLN3* may inhibit disproportionately its translational efficiency in poor media
314 (POLYMENIS AND SCHMIDT 1997). However, such predictions have not been accompanied with
315 measurements of Cln3p levels. A kinetic model of protein synthesis (LODISH 1974) forecasts that
316 removing the uORF would de-repress synthesis of Cln3p in low growth rates when the ribosome content
317 of the cell is low. In contrast, removing the *CLN3* uORF would have minimal effects in cells that
318 proliferate fast, when the ribosome content is high. To test this model, we introduced an A-315T
319 substitution that mutates the start codon of the uORF in *CLN3* without affecting *CLN3* mRNA levels
320 (POLYMENIS AND SCHMIDT 1997), in the strain that expresses otherwise wild type Whi5p-TAP and Cln3p-
321 $(Myc)_{13}$ (see Materials and Methods). Indeed, in *CLN3* uORF mutant cells proliferating slower (T_d > 4h),
322 the dynamic range of Cln3p levels as a function of growth rate was narrower and indistinguishable from
323 the range of Whi5p levels (Figure 4A, B and Source Data). A hallmark phenotypic readout of gain-of-
324 function *CLN3* alleles is a reduction in cell size (NASH *et al.* 1988). Consistent with a de-repression of
325 Cln3p synthesis, not only cells that lack the *CLN3* uORF were smaller than their wild type counterparts
326 were, but also this effect was growth rate-dependent (see Figure 4C, D) in glucose and especially in
327 leucine-limited cells, with the latter displaying pronounced enlargement that was suppressed by

328 removing the *CLN3* uORF. These data argue that translational control contributes to the
329 disproportionate reduction of Cln3p levels as a function of growth rate. Overall, higher Cln3p levels, by
330 stabilizing the protein or by de-repressing Cln3p synthesis via translational control, alter the slope of the
331 linear relation between T_d and T_{G1} (see Table 1). Conversely, loss of Cln3p severely perturbs the linear
332 relation altogether (Figure 3). These results underscore the critical role of the G1 cyclin Cln3p in the
333 physiological coupling between growth and division.

334 **DISCUSSION**

335 The scaling relations between G1 length and population time in yeast and human cells we report are
336 important for several reasons. First, if the duration of G1 is estimated, they allow predictions of
337 proliferation rates, which could be useful in diverse settings, such as in tissues at an organismal level.
338 Second, they serve as benchmarks against which the effects of genetic or other perturbations can be
339 evaluated, as we demonstrated for Whi5p and Cln3p, two cell cycle regulators in yeast. Third, scaling
340 relations of cellular physiology may ultimately point to general, physical mechanisms that organize life at
341 the cellular level.

342 How do the results we report here impinge on the Whi5p dilution model (SCHMOLLER *et al.* 2015),
343 which was reported to account for the coupling between growth and division in budding yeast? As we
344 noted above, our data dealt with growth rate-dependent changes in the cell cycle, which was not
345 addressed in (SCHMOLLER *et al.* 2015). Hence, the two studies are not directly comparable. A critical
346 aspect of the Whi5p dilution model, however, was that while Whi5p levels were disproportionately
347 lower than expected from cell growth, Cln3p levels were roughly constant and proportional to the
348 increase in size from birth to START (SCHMOLLER *et al.* 2015). Given the strong and disproportionate
349 dependency of Cln3p levels on growth rate that we report here and had predicted earlier (POLYMENIS AND
350 SCHMIDT 1997), could the uORF-mediated translational control of *CLN3* affect Cln3p synthesis in the G1
351 phase from birth to START? We think this is unlikely because the uORF-mediated translational control
352 we described operates when the concentration of active ribosomes in the cell changes (LODISH 1974), for
353 example in poor vs. rich nutrients. To our knowledge, there is no report of cell cycle-dependent changes
354 in ribosome content.

355 Other mechanisms may contribute to significant changes in Cln3p abundance in G1, which could
356 have implications for the Whi5p dilution model. There are conflicting reports in the literature about
357 whether Cln3p 'cycles' in the cell cycle. The initial report claiming that Cln3p levels are constant in the

358 cell cycle did not interrogate the early G1 phase (TYERS *et al.* 1993). In that report, although early G1,
359 small (25 fL), elutriated daughter cells were collected, Cln3p levels were not measured until much later
360 in G1 (at 35 fL, when by 40 fL 25% of the cells were already budded; see Fig. 4 in (TYERS *et al.* 1993)).
361 Based on that result, it had been assumed for decades that Cln3p levels were constant in the cell cycle.
362 Cln3p abundance cannot be properly addressed in the single-cell microscopy methods of (SCHMOLLER *et*
363 *al.* 2015), because a mutated *CLN3* allele had to be used, producing a stabilized Cln3p protein so that it
364 can accumulate at high enough, but non-physiological levels to be visible with microscopy. Recently,
365 however, two independent studies by the Kellogg (ZAPATA *et al.* 2014) and Amon (THORBURN *et al.* 2013)
366 labs, assayed elutriated synchronous cells carrying epitope-tagged, but otherwise wild type *CLN3* alleles.
367 Both studies showed that Cln3p levels oscillate >10-fold in G1. Cln3p is absent in early G1 cells, while it
368 rises dramatically before START. Hence, although a 2-fold dilution of Whi5p is observed in G1 (SCHMOLLER
369 *et al.* 2015), the changes in Cln3p levels are likely more pronounced (THORBURN *et al.* 2013; ZAPATA *et al.*
370 2014), through transcriptional (ZAPATA *et al.* 2014), or other mechanisms. It is important to stress,
371 however, those changes of Cln3p levels in G1 do not affect the fundamental aspect of the inhibitor
372 dilution model, namely that Whi5p levels are reduced by cell growth. Instead, we may be dealing with a
373 more complex, 'mixed' model of inhibitor dilution *and* activator accumulation.

ACKNOWLEDGEMENTS

Author Contributions: Methodology, H.M.B., M.P.; Formal Analysis, H.M.B., M.P.; Investigation, H.M.B., M.C., I.P.E.P., A.O.P., M.P.; Resources, M.P.; Data Curation, H.M.B., M.P.; Writing – Original Draft, M.P., Writing – Review and Editing, H.M.B., M.P.; Visualization, H.M.B., M.P.; Supervision, H.M.B., M.P., Funding Acquisition, M.P.

This work was supported from the NIH (grant GM123139 to M.P.). M.C. was supported by a National Science Foundation REU award (DBI-1358941). The authors declare no conflicts of interest.

381 **LITERATURE CITED**

382 Amir, A., 2017 Is cell size a spandrel? Elife 6.

383 Anastasia, S. D., D. L. Nguyen, V. Thai, M. Meloy, T. MacDonough *et al.*, 2012 A link between mitotic
384 entry and membrane growth suggests a novel model for cell size control. J Cell Biol 197**:** 89-104.

385 Aoki, Y., and G. E. Moore, 1970 Comparative study of mitotic stages of cells derived from human
386 peripheral blood. Exp Cell Res 59**:** 259-266.

387 Baserga, R., 1985 *The Biology of Cell Reproduction*.

388 Blank, H. M., R. Perez, C. He, N. Maitra, R. Metz *et al.*, 2017 Translational control of lipogenic enzymes in
389 the cell cycle of synchronous, growing yeast cells. EMBO J 36**:** 487-502.

390 Brauer, M. J., C. Huttenhower, E. M. Airoldi, R. Rosenstein, J. C. Matese *et al.*, 2008 Coordination of
391 growth rate, cell cycle, stress response, and metabolic activity in yeast. Mol Biol Cell 19**:** 352-
392 367.

393 Brons, P. P., J. M. Raemaekers, M. J. Bogman, P. E. van Erp, J. B. Boezeman *et al.*, 1992 Cell cycle kinetics
394 in malignant lymphoma studied with in vivo iododeoxyuridine administration, nuclear Ki-67
395 staining, and flow cytometry. Blood 80**:** 2336-2343.

396 Brunner, N., D. Bronzert, L. L. Vindelov, K. Rygaard, M. Spang-Thomsen *et al.*, 1989 Effect on growth and
397 cell cycle kinetics of estradiol and tamoxifen on MCF-7 human breast cancer cells grown in vitro
398 and in nude mice. Cancer Res 49**:** 1515-1520.

399 Bryan, A. K., A. Engler, A. Gulati and S. R. Manalis, 2012 Continuous and long-term volume
400 measurements with a commercial Coulter counter. PLoS One 7**:** e29866.

401 Calder, W. A., 3rd, 1981 Scaling of physiological processes in homeothermic animals. Annu Rev Physiol
402 43**:** 301-322.

403 Carter, B. L., and M. N. Jagadish, 1978 Control of cell division in the yeast Saccharomyces cerevisiae
404 cultured at different growth rates. Exp Cell Res 112**:** 373-383.

405 Cerulus, B., A. M. New, K. Pougach and K. J. Verstrepen, 2016 Noise and Epigenetic Inheritance of Single-
406 Cell Division Times Influence Population Fitness. Curr Biol 26: 1138-1147.
407 Chan, Y. H., and W. F. Marshall, 2010 Scaling properties of cell and organelle size. Organogenesis 6: 88-
408 96.
409 Costanzo, M., J. L. Nishikawa, X. Tang, J. S. Millman, O. Schub *et al.*, 2004 CDK activity antagonizes Whi5,
410 an inhibitor of G1/S transcription in yeast. Cell 117: 899-913.
411 Cross, F. R., 1988 DAF1, a mutant gene affecting size control, pheromone arrest, and cell cycle kinetics of
412 Saccharomyces cerevisiae. Mol Cell Biol 8: 4675-4684.
413 de Bruin, R. A., W. H. McDonald, T. I. Kalashnikova, J. Yates, 3rd and C. Wittenberg, 2004 Cln3 activates
414 G1-specific transcription via phosphorylation of the SBF bound repressor Whi5. Cell 117: 887-
415 898.
416 Defendi, V., and L. A. Manson, 1963 Analysis of the life-cycle in mammalian cells. Nature 198: 359-361.
417 Di Talia, S., J. M. Skotheim, J. M. Bean, E. D. Siggia and F. R. Cross, 2007 The effects of molecular noise
418 and size control on variability in the budding yeast cell cycle. Nature 448: 947-951.
419 Dowling, M. R., A. Kan, S. Heinzel, J. H. Zhou, J. M. Marchingo *et al.*, 2014 Stretched cell cycle model for
420 proliferating lymphocytes. Proc Natl Acad Sci U S A 111: 6377-6382.
421 Elliott, S. G., and C. S. McLaughlin, 1978 Rate of macromolecular synthesis through the cell cycle of the
422 yeast Saccharomyces cerevisiae. Proc Natl Acad Sci U S A 75: 4384-4388.
423 Ferrezuelo, F., N. Colomina, A. Palmisano, E. Gari, C. Gallego *et al.*, 2012 The critical size is set at a single-
424 cell level by growth rate to attain homeostasis and adaptation. Nat Commun 3: 1012.
425 Fisher, R. P., 2016 Getting to S: CDK functions and targets on the path to cell-cycle commitment.
426 F1000Research 5: 2374.
427 Garner, K. M., and A. Eastman, 2011 Variations in Mre11/Rad50/Nbs1 status and DNA damage-induced
428 S-phase arrest in the cell lines of the NCI60 panel. BMC Cancer 11: 206:201-213.

429 Guo, J., B. A. Bryan and M. Polymenis, 2004 Nutrient-specific effects in the coordination of cell growth
430 with cell division in continuous cultures of Saccharomyces cerevisiae. Arch Microbiol 182: 326-
431 330.
432 Hahn, A. T., J. T. Jones and T. Meyer, 2009 Quantitative analysis of cell cycle phase durations and PC12
433 differentiation using fluorescent biosensors. Cell Cycle 8: 1044-1052.
434 Hartwell, L. H., and M. W. Unger, 1977 Unequal division in Saccharomyces cerevisiae and its implications
435 for the control of cell division. J Cell Biol 75: 422-435.
436 Henry, K. A., H. M. Blank, S. A. Hoose and M. Polymenis, 2010 The unfolded protein response is not
437 necessary for the G1/S transition, but it is required for chromosome maintenance in
438 Saccharomyces cerevisiae. PLoS One 5: e12732.
439 Hoffman, J. G., 1949 Theory of the mitotic index and its application to tissue growth measurement. Bull
440 Math Biophys 11: 139-144.
441 Hoose, S. A., J. A. Rawlings, M. M. Kelly, M. C. Leitch, Q. O. Ababneh *et al.*, 2012 A systematic analysis of
442 cell cycle regulators in yeast reveals that most factors act independently of cell size to control
443 initiation of division. PLoS Genet 8: e1002590.
444 Hoose, S. A., J. T. Trinh, M. C. Leitch, M. M. Kelly, R. F. McCormick *et al.*, 2013 Saccharomyces cerevisiae
445 deletion strains with complex DNA content profiles. FEMS Microbiol Lett 345: 72-76.
446 Jagadish, M. N., and B. L. Carter, 1977 Genetic control of cell division in yeast cultured at different
447 growth rates. Nature 269: 145-147.
448 Johnston, G., R. Singer, S. Sharrow and M. Slater, 1980 Cell division in the yeast Saccharomyces
449 cerevisiae growing at different rates. Microbiology 118: 479-484.
450 Johnston, G. C., J. R. Pringle and L. H. Hartwell, 1977 Coordination of growth with cell division in the
451 yeast Saccharomyces cerevisiae. Exp Cell Res 105: 79-98.

452 Koch, A. L., 1966 The logarithm in biology. 1. Mechanisms generating the log-normal distribution exactly.
453 J Theor Biol 12: 276-290.
454 Koch, A. L., and M. Schaechter, 1962 A model for statistics of the cell division process. J Gen Microbiol
455 29: 435-454.
456 Kumei, Y., T. Nakajima, A. Sato, N. Kamata and S. Enomoto, 1989 Reduction of G1 phase duration and
457 enhancement of c-myc gene expression in HeLa cells at hypergravity. Journal of Cell Science 93:
458 221-226.
459 Lennartz, K. J., and W. Maurer, 1964 Autoradiographische Bestimmung der Dauer der DNS-Verdopplung
460 und der Generationszeit beim Ehrlich-Ascitestumor der Maus durch Doppelmarkierung mit 14C-
461 und 3H-Thymidin. Zeitschrift für Zellforschung und Mikroskopische Anatomie 63: 478-495.
462 Liu, X., X. Wang, X. Yang, S. Liu, L. Jiang *et al.*, 2015 Reliable cell cycle commitment in budding yeast is
463 ensured by signal integration. Elife 4.
464 Lodish, H. F., 1974 Model for the regulation of mRNA translation applied to haemoglobin synthesis.
465 Nature 251: 385-388.
466 Luciani, A. M., A. Rosi, P. Matarrese, G. Arancia, L. Guidoni *et al.*, 2001 Changes in cell volume and
467 internal sodium concentration in HeLa cells during exponential growth and following lonidamine
468 treatment. Eur J Cell Biol 80: 187-195.
469 Mayhew, M. B., E. S. Iversen and A. J. Hartemink, 2017 Characterization of dependencies between
470 growth and division in budding yeast. J R Soc Interface 14.
471 Morgan, D. O., 2007 Control of Cell Proliferation and Growth, pp. 221 in *The Cell Cycle*. New Science
472 Press Ltd, London, UK.
473 Nash, R., G. Tokiwa, S. Anand, K. Erickson and A. B. Futcher, 1988 The WHI1+ gene of Saccharomyces
474 cerevisiae tethers cell division to cell size and is a cyclin homolog. EMBO J 7: 4335-4346.

475 Palumbo, P., M. Vanoni, V. Cusimano, S. Busti, F. Marano *et al.*, 2016 Whi5 phosphorylation embedded
476 in the G1/S network dynamically controls critical cell size and cell fate. 7**:** 11372.
477 Pena, E. A., and E. H. Slate, 2006 Global Validation of Linear Model Assumptions. J Am Stat Assoc 101**:**
478 341.
479 Polymenis, M., and E. V. Schmidt, 1997 Coupling of cell division to cell growth by translational control of
480 the G1 cyclin CLN3 in yeast. Genes Dev 11**:** 2522-2531.
481 Rivin, C. J., and W. L. Fangman, 1980 Cell cycle phase expansion in nitrogen-limited cultures of
482 Saccharomyces cerevisiae. J Cell Biol 85**:** 96-107.
483 Ross, D. T., U. Scherf, M. B. Eisen, C. M. Perou, C. Rees *et al.*, 2000 Systematic variation in gene
484 expression patterns in human cancer cell lines. Nat Genet 24**:** 227-235.
485 Schaechter, M., O. Maaloe and N. O. Kjeldgaard, 1958 Dependency on medium and temperature of cell
486 size and chemical composition during balanced grown of Salmonella typhimurium. J Gen
487 Microbiol 19**:** 592-606.
488 Scherf, U., D. T. Ross, M. Waltham, L. H. Smith, J. K. Lee *et al.*, 2000 A gene expression database for the
489 molecular pharmacology of cancer. Nat Genet 24**:** 236-244.
490 Schmoller, K. M., and J. M. Skotheim, 2015 The Biosynthetic Basis of Cell Size Control. Trends Cell Biol
491 25**:** 793-802.
492 Schmoller, K. M., J. J. Turner, M. Koivomagi and J. M. Skotheim, 2015 Dilution of the cell cycle inhibitor
493 Whi5 controls budding-yeast cell size. Nature 526**:** 268-272.
494 Si, F., D. Li, S. E. Cox, J. T. Sauls, O. Azizi *et al.*, 2017 Invariance of Initiation Mass and Predictability of Cell
495 Size in Escherichia coli. Curr Biol 27**:** 1278-1287.
496 Siegel, A. F., 1982 Robust regression using repeated medians. Biometrika 69**:** 242-244.
497 Sisken, J. E., and R. Kinosita, 1961 TIMING OF DNA SYNTHESIS IN THE MITOTIC CYCLE IN VITRO. J Biophys
498 Biochem Cytol 9**:** 509-518.

499 Slater, M. L., S. O. Sharrow and J. J. Gart, 1977 Cell cycle of Saccharomycescerevisiae in populations
500 growing at different rates. Proc Natl Acad Sci U S A 74: 3850-3854.
501 Soifer, I., and N. Barkai, 2014 Systematic identification of cell size regulators in budding yeast. Molecular
502 systems biology 10.
503 Soma, S., K. Yang, M. I. Morales and M. Polymenis, 2014 Multiple metabolic requirements for size
504 homeostasis and initiation of division in Saccharomyces cerevisiae. Microb Cell 1: 256-266.
505 Son, S., A. Tzur, Y. Weng, P. Jorgensen, J. Kim *et al.*, 2012 Direct observation of mammalian cell growth
506 and size regulation. Nature methods 9: 910-912.
507 Thorburn, R. R., C. Gonzalez, G. A. Brar, S. Christen, T. M. Carlile *et al.*, 2013 Aneuploid yeast strains
508 exhibit defects in cell growth and passage through START. Mol Biol Cell 24: 1274-1289.
509 Tyers, M., G. Tokiwa and B. Futcher, 1993 Comparison of the Saccharomyces cerevisiae G1 cyclins: Cln3
510 may be an upstream activator of Cln1, Cln2 and other cyclins. Embo j 12: 1955-1968.
511 Tyson, C. B., P. G. Lord and A. E. Wheals, 1979 Dependency of size of Saccharomyces cerevisiae cells on
512 growth rate. J Bacteriol 138: 92-98.
513 Zapata, J., N. Dephoure, T. Macdonough, Y. Yu, E. J. Parnell *et al.*, 2014 PP2ARts1 is a master regulator of
514 pathways that control cell size. J Cell Biol 204: 359-376.

515

516 **FIGURE LEGENDS**

517 **FIGURE 1. Linking the length of the G1 phase with population doubling time.** Scatter plots of T_{G1} (**A, C**)
518 or T_{nonG1} (**B, D**) values on the x-axis, against T_d values (y-axis). All plots used the natural logarithms of the
519 values for yeast (**A, B**) and human (**C, D**) cells from Tables S1 and S2, respectively. The Kendall's (τ) rank
520 correlation coefficient is shown in each case. In red are regression lines of the Siegel repeated medians.
521 The slope and the associated 95% confidence intervals of the linear model are shown in each case.
522 Additional statistical parameters associated with these plots are shown in Table 1.

523

524 **FIGURE 2. Cell size does not correlate with T_d or T_{G1} in yeast.** Scatter plots of cell size values (x-axis)
525 against T_d (**A**) or T_{G1} (**B**) values (y-axis) from the data shown in Table S1. In red are regression lines of the
526 Siegel repeated medians. The Kendall's (τ) and Spearman's (r) rank correlation coefficients are shown in
527 each case.

528

529 **FIGURE 3. Cln3p, but not Whi5p, imposes the proper relation between T_{G1} and T_d.** Scatter plots of T_{G1}
530 values on the x-axis, against T_d values (y-axis). All plots used the natural logarithms of the values for
531 *whi5Δ* (**A**) or *cln3Δ* (**B**) cells, sampled from chemostat cultures several times at each dilution rate, as
532 indicated. In red are regression lines of the Siegel repeated medians. For *whi5Δ* cells, the slope of the
533 linear model is shown (additional statistical parameters are in Table 1). For *cln3Δ* cells, the linear fit is
534 shown in dashed form and did not include Ln(T_d) values >2.0, because the relation between T_d and T_{G1}
535 breaks down at those proliferation rates for those cells. Scatter plots of the relation of cell size and T_d in
536 cells lacking Whip5 (**C**) or Cln3p (**D**), with cell size values (x-axis) plotted against T_d (y-axis) from the same
537 cultures described in (**A**) and (**B**).

538

539 **FIGURE 4. The levels of the G1 cyclin Cln3p vary over a broad range as a function of growth rate, due**
540 **to a uORF affecting translation of *CLN3*.** Scatter plots of the relative abundance (y-axis) of Cln3p-$(Myc)_{13}$
541 and Whi5p-TAP in otherwise wild type *CLN3-13MYC*, *WHI5-TAP* cells (**A**), or *CLN3* uORF (*A-315T-CLN3*)
542 mutant cells (**B**), against T_d (x-axis). Each data point in the scatter plots is the average of immunoblot
543 signal intensities run in duplicate, and detected with antibodies against the Myc or TAP epitopes (see
544 Materials and Methods). All the raw immunoblots used to quantify protein levels are shown in the
545 Source Data (Supplementary File 1). Before averaging, each individual signal intensity value was
546 normalized against loading in the corresponding immunoblot lane (visualized with Ponceau staining, see
547 Supplementary File 1 and Materials and Methods). For each Cln3p-$(Myc)_{13}$ or Whi5p-TAP relative unit
548 (r.u.) shown in the scatterplots (**A, B**), the normalized, averaged intensities were scaled by the lowest
549 value (set to 1) for each protein in the given chemostat experiment run at different dilution rates.
550 Scatter plots of the relation of cell size (x-axis) and T_d (y-axis) in the indicated strains, cultured under
551 glucose (**C**) or leucine (**D**) limitation, from the same cultures described in (**A**) and (**B**).

552 **TABLE 1. Statistical parameters of linear relations**

Variables		Coefficients[a]		Confidence Intervals (level = 0.95)[b]				τ[c]	r[d]
Y	X	Intercept	Slope	Intercept		Slope			
$(T_d)_{yeast}$	$(T_{G1})_{yeast}$	1.429	1.091	1.3817	1.5049	1.0598	1.1133	0.815	0.938
$(T_d)_{yeast}$	$(T_{nonG1})_{yeast}$	0.36	1.75	0.1900	0.8712	1.6244	2.0278	0.398	0.532
$Ln(T_d)_{yeast}$	$Ln(T_{G1})_{yeast}$	0.9168	0.5955	0.9047	0.9418	0.5815	0.6136	0.815	0.938
$Ln(T_d)_{yeast}$	$Ln(T_{nonG1})_{yeast}$	0.8682	0.8745	0.7764	0.9128	0.7827	0.9659	0.398	0.532
$(T_d)_{human}$	$(T_{G1})_{human}$	7.558	1.279	6.8401	8.5971	1.2433	1.3339	0.775	0.921
$(T_d)_{human}$	$(T_{nonG1})_{human}$	6.838	1.738	3.6212	7.3905	1.6919	2.0059	0.579	0.762
$Ln(T_d)_{human}$	$Ln(T_{G1})_{human}$	1.2202	0.7656	1.1770	1.3663	0.7211	0.7843	0.775	0.921
$Ln(T_d)_{human}$	$Ln(T_{nonG1})_{human}$	1.3608	0.7816	1.1374	1.4674	0.7487	0.8762	0.579	0.762
$Ln(T_d)_{whi5\Delta}$[e]	$Ln(T_{G1})_{whi5\Delta}$[e]	1.1654	0.6166	1.1613	1.1910	0.6083	0.6362	0.928	0.987
$Ln(T_d)_{HB94/7}$[f]	$Ln(T_{G1})_{HB94/7}$	0.9691	0.6848	0.9031	0.9843	0.6588	0.7461	0.765	0.918
$Ln(T_d)_{HB104}$[g]	$Ln(T_{G1})_{HB104}$	0.9913	0.7048	0.9902	1.0074	0.6930	0.7120	0.934	0.989

553

554 [a]From the linear fit of Siegel repeated medians, calculated with the 'mblm' function of the *mblm* R

555 package.

556 [b]Calculated with the 'confint.mblm' function of the *mblm* R package.

557 [c]Kendall's (τ) rank correlation coefficient, calculated with the 'cor.test' function of the *stats* R package.

558 [d]Spearman's (r) rank correlation coefficient, calculated with the 'cor.test' function of the *stats* R

559 package.

560 [e]The values for *whi5Δ* cells were from the experiment shown in Figure 3A.

561 [f]The values for HB94/7 cells (*CLN3-13MYC*, *WHI5-TAP*) were from the experiments in Figure 4A.

562 [g]The values for HB104 cells (*A-315T-CLN3-13MYC*, *WHI5-TAP*) were from the experiments in Figure 4B.

563 **SUPPLEMENTARY INFORMATION**

564 **SUPPLEMENTARY FIGURE LEGENDS**

565 **FIGURE S1. Goodness-of-fit plots for log-normal distribution of yeast (A-D), and human (E-H), T_{G1}**
566 **values, from Tables S1, and S2, respectively. A, E.** Histogram of experimental T_{G1} values, with the
567 theoretical log-normal density plot shown in red. **B, F.** Plot of the cumulative distribution function (CDF)
568 of experimental T_{G1} values (shown as open symbols), along with the theoretical CDF of the log-normal
569 distribution (shown in red). **C, G.** Quantile-Quantile (Q-Q) plot, comparing the experimental quantiles of
570 T_{G1} values (shown as open symbols) against the theoretical quantiles of a log-normal distribution (shown
571 as the diagonal line). Q-Q plots emphasize poor fit at the tails of the distribution. **D, H.** Probability-
572 Probability (P–P) plot of the CDF of experimental T_{G1} values plotted against the theoretical CDF of the
573 log-normal distribution (shown as the diagonal line). P-P plots emphasize poor fit at the center of the
574 distribution. The plots were generated with the *fitdistrplus* R package.

575

576 **FIGURE S2. Diagnostic plots of simple linear regression models for T_d and T_{G1} values of yeast (A-D), and**
577 **human (E-H), cells.** The log-transformed T_d and T_{G1} values shown in Tables S1 and S2 were used to build
578 simple linear regression models with the 'lm' function of the *stats* R package. **A, E**. Plot of residuals (y-
579 axis) against fitted values (x-axis). Numbered data points indicate problematic outliers. **B, F**. Normal Q-Q
580 plot of the ordered standardized residuals (y-axis), against the expected order statistics from a standard
581 normal distribution (x-axis). Points away from the straight dashed line indicate departures from
582 normality. **C, G**. Scale-Location plot of the square root of the absolute residuals (y-axis) against fitted
583 values (x-axis), in order to diminish skewness. **D, H**. Plot of residuals (y-axis) against leverages (x-axis).
584 The residual-leverage plot shows contours (shown with dashed red lines) of equal Cook's distance (by
585 default 0.5 and 1). Plots in **B, C, D, F, G, H** use standardized residuals which have identical variance

(under the hypothesis of normality). The solid red lines in **A, C, D, E, G, H** indicate the locally weighted scatterplot smoothing.

588 **Table S1. *S. cerevisiae* cell cycle kinetics in different media**

Culture medium	Cell size (fL)	T_d (h)	T_{G1} (h)	Reference
YP+Dextrose	34.3	1.3	0.3	(TYSON *et al.* 1979)
YP+Fructose	36.6	1.3	0.3	(TYSON *et al.* 1979)
YP+Sucrose	38.7	1.3	0.3	(TYSON *et al.* 1979)
YP+Dextrose		1.4	0.3	(SLATER *et al.* 1977)
MM2+Fructose	34	1.5	0.4	(TYSON *et al.* 1979)
MM2+Dextrose	25.9	1.6	0.5	(TYSON *et al.* 1979)
YP+Raffinose		1.7	0.4	This study
YP+Dextrose		1.7	0.5	This study
YP+Raffinose	18	1.8	0.6	(TYSON *et al.* 1979)
MM+Dextrose+Ammonia		1.8	0.9	(RIVIN AND FANGMAN 1980)
MM+Dextrose+Glutamine		1.8	1.0	(RIVIN AND FANGMAN 1980)
MM1+Dextrose	17.8	2.0	0.7	(TYSON *et al.* 1979)
MM1+Maltose	25.5	2.0	0.7	(TYSON *et al.* 1979)
MM1+Fructose	22.8	2.1	0.8	(TYSON *et al.* 1979)
YP+Maltose	21.2	2.1	0.9	(TYSON *et al.* 1979)
SF		2.2	0.7	(SLATER *et al.* 1977)
YP+Glycerol		2.2	0.7	This study
YP+Ethanol		2.2	0.8	This study
Glucose-limited chemostat	38.8	2.3	0.5	(BRAUER *et al.* 2008)
Leucine-limited chemostat	27.6	2.3	0.7	(BRAUER *et al.* 2008)
Uracil-limited chemostat	41	2.3	0.7	(BRAUER *et al.* 2008)
Phosphorous-limited chemostat	46.3	2.3	0.8	(BRAUER *et al.* 2008)
YP+Sorbitol	15.9	2.3	0.8	(TYSON *et al.* 1979)
YP+Galactose		2.3	0.8	This study
Nitrogen-limited chemostat	30.6	2.3	1	(BRAUER *et al.* 2008)
Sulfur-limited chemostat	29.9	2.3	1	(BRAUER *et al.* 2008)
Glucose-limited chemostat	18.9	2.3	1	(GUO *et al.* 2004)
Nitrogen-limited chemostat	30	2.3	1	(GUO *et al.* 2004)
Glucose-limited chemostat		2.3	1.5	(HENRY *et al.* 2010)
Nitrogen-limited chemostat		2.3	1.5	(HENRY *et al.* 2010)
Nitrogen-limited chemostat		2.3	1.6	(HENRY *et al.* 2010)
Nitrogen-limited chemostat		2.3	1.6	(HENRY *et al.* 2010)
Nitrogen-limited chemostat		2.3	2.1	(HENRY *et al.* 2010)
YP+Gluconate	25.8	2.4	0.6	(TYSON *et al.* 1979)
MM+Dextrose+Glutamate		2.4	0.7	(JOHNSTON *et al.* 1980)
MM+Dextrose+Ammonia		2.6	0.9	(JOHNSTON *et al.* 1980)
YP+Galactose	21.5	2.6	1.1	(TYSON *et al.* 1979)
Glucose-limited chemostat		2.7	0.3	(JAGADISH AND CARTER 1977)
Glucose-limited chemostat		2.7	0.4	(JAGADISH AND CARTER 1977)
YP+Glycerol	24.1	2.7	1.2	(TYSON *et al.* 1979)
Uracil-limited chemostat	37.3	2.8	0.7	(BRAUER *et al.* 2008)
Glucose-limited chemostat	33.6	2.8	1	(BRAUER *et al.* 2008)
YP+Dextrose		2.8	1.0	(JAGADISH AND CARTER 1977)

Nitrogen-limited chemostat	23.9	2.8	1.1	(BRAUER *et al.* 2008)
Nitrogen-limited chemostat	29.9	2.8	1.1	(GUO *et al.* 2004)
Leucine-limited chemostat	36.6	2.8	1.2	(BRAUER *et al.* 2008)
Phosphorous-limited chemostat	37.3	2.8	1.2	(BRAUER *et al.* 2008)
Glucose-limited chemostat	19	2.8	1.3	(GUO *et al.* 2004)
Sulfur-limited chemostat	26.1	2.8	1.5	(BRAUER *et al.* 2008)
Glucose-limited chemostat		2.8	1.8	(HENRY *et al.* 2010)
Nitrogen-limited chemostat		2.8	1.8	(HENRY *et al.* 2010)
Nitrogen-limited chemostat		2.8	1.8	(HENRY *et al.* 2010)
Nitrogen-limited chemostat		2.8	1.9	(HENRY *et al.* 2010)
Nitrogen-limited chemostat		2.8	2.1	(HENRY *et al.* 2010)
Nitrogen-limited chemostat		2.8	2.2	(HENRY *et al.* 2010)
Glucose-limited chemostat		2.9	0.7	(CARTER AND JAGADISH 1978)
YP+Dextrose		3	0.8	(CARTER AND JAGADISH 1978)
YP+Mannitol	20	3.2	1.0	(TYSON *et al.* 1979)
YP+Trehalose	17.8	3.2	1.0	(TYSON *et al.* 1979)
MM3+Acetate	21.6	3.2	1.1	(TYSON *et al.* 1979)
Glucose-limited chemostat		3.2	1.2	(CARTER AND JAGADISH 1978)
MM+Dextrose+Proline		3.3	1.4	(JAGADISH AND CARTER 1977)
MM+Dextrose+Ammonia+CHX		3.3	1.6	(HARTWELL AND UNGER 1977)
SEY		3.3	1.7	(SLATER *et al.* 1977)
MM+Dextrose+Methionine		3.3	1.9	(RIVIN AND FANGMAN 1980)
Glucose-limited chemostat		3.5	1.1	(JAGADISH AND CARTER 1977)
Nitrogen-limited chemostat	29.3	3.5	1.3	(GUO *et al.* 2004)
Leucine-limited chemostat	35.1	3.5	1.5	(BRAUER *et al.* 2008)
Uracil-limited chemostat	41	3.5	1.5	(BRAUER *et al.* 2008)
Phosphorous-limited chemostat	32.1	3.5	1.7	(BRAUER *et al.* 2008)
Glucose-limited chemostat	17.9	3.5	1.8	(GUO *et al.* 2004)
Glucose-limited chemostat	32.1	3.5	1.9	(BRAUER *et al.* 2008)
Sulfur-limited chemostat	26.9	3.5	2	(BRAUER *et al.* 2008)
Nitrogen-limited chemostat	24	3.5	2.1	(BRAUER *et al.* 2008)
Nitrogen-limited chemostat		3.5	2.1	(HENRY *et al.* 2010)
Nitrogen-limited chemostat		3.5	2.3	(HENRY *et al.* 2010)
Nitrogen-limited chemostat		3.5	2.5	(HENRY *et al.* 2010)
Nitrogen-limited chemostat		3.5	2.8	(HENRY *et al.* 2010)
Glucose-limited chemostat		3.5	2.9	(HENRY *et al.* 2010)
Nitrogen-limited chemostat		3.5	2.9	(HENRY *et al.* 2010)
MM+Dextrose+Proline		3.8	1.6	(CARTER AND JAGADISH 1978)
Glucose-limited chemostat		3.9	1.4	(JAGADISH AND CARTER 1977)
MM+Dextrose+Leucine		4	1.8	(JOHNSTON *et al.* 1980)
Nitrogen-limited chemostat		4	3.1	(HENRY *et al.* 2010)
Glucose-limited chemostat		4.2	1.8	(CARTER AND JAGADISH 1978)
Glucose-limited chemostat		4.3	2.1	(CARTER AND JAGADISH 1978)
SE		4.3	2.4	(SLATER *et al.* 1977)
MM+Dextrose+Threonine		4.3	2.6	(RIVIN AND FANGMAN 1980)
EMM+Galactose	22.9	4.5	2.2	(TYSON *et al.* 1979)

Uracil-limited chemostat	41.8	4.6	2	(BRAUER *et al.* 2008)
Nitrogen-limited chemostat	29.6	4.6	2	(GUO *et al.* 2004)
Phosphorous-limited chemostat	31.3	4.6	2.3	(BRAUER *et al.* 2008)
Glucose-limited chemostat		4.6	2.3	(JAGADISH AND CARTER 1977)
Glucose-limited chemostat	29.9	4.6	2.6	(BRAUER *et al.* 2008)
Glucose-limited chemostat	19	4.6	2.6	(GUO *et al.* 2004)
Leucine-limited chemostat	38.1	4.6	2.9	(BRAUER *et al.* 2008)
Nitrogen-limited chemostat		4.6	3.1	(HENRY *et al.* 2010)
Sulfur-limited chemostat	27.6	4.6	3.2	(BRAUER *et al.* 2008)
Nitrogen-limited chemostat	23.9	4.6	3.5	(BRAUER *et al.* 2008)
Nitrogen-limited chemostat		4.6	3.5	(HENRY *et al.* 2010)
Nitrogen-limited chemostat		4.6	3.6	(HENRY *et al.* 2010)
Nitrogen-limited chemostat		4.6	3.8	(HENRY *et al.* 2010)
Nitrogen-limited chemostat		4.6	3.9	(HENRY *et al.* 2010)
Glucose-limited chemostat		4.6	4	(HENRY *et al.* 2010)
MM1+Glycerol	16.9	4.9	3.1	(TYSON *et al.* 1979)
YP+Glycerol		5.2	3.0	(CARTER AND JAGADISH 1978)
YP+Glycerol		5.2	3.2	(JAGADISH AND CARTER 1977)
MM+Dextrose+Ammonia+CHX		5.4	3.6	(HARTWELL AND UNGER 1977)
MM+Dextrose+Tryptophan		5.6	3.8	(JOHNSTON *et al.* 1980)
Glucose-limited chemostat		6.2	2.6	(JAGADISH AND CARTER 1977)
Glucose-limited chemostat		6.2	3.9	(JAGADISH AND CARTER 1977)
MM4+Acetate	19.5	6.4	3.4	(TYSON *et al.* 1979)
MM+Dextrose+Proline		6.4	4.5	(JOHNSTON *et al.* 1980)
Glucose-limited chemostat		6.6	4.5	(CARTER AND JAGADISH 1978)
MM+Dextrose+Proline		6.7	4.7	(RIVIN AND FANGMAN 1980)
Nitrogen-limited chemostat	33.2	6.9	3	(GUO *et al.* 2004)
Glucose-limited chemostat	18.9	6.9	4.3	(GUO *et al.* 2004)
Glucose-limited chemostat	36.6	6.9	4.4	(BRAUER *et al.* 2008)
Nitrogen-limited chemostat		6.9	4.8	(HENRY *et al.* 2010)
Uracil-limited chemostat	47.8	6.9	5	(BRAUER *et al.* 2008)
Phosphorous-limited chemostat	40.3	6.9	5.1	(BRAUER *et al.* 2008)
Nitrogen-limited chemostat		6.9	5.1	(HENRY *et al.* 2010)
Leucine-limited chemostat	38.1	6.9	5.3	(BRAUER *et al.* 2008)
Sulfur-limited chemostat	27.6	6.9	5.3	(BRAUER *et al.* 2008)
Nitrogen-limited chemostat	29.9	6.9	5.5	(BRAUER *et al.* 2008)
Nitrogen-limited chemostat		6.9	5.8	(HENRY *et al.* 2010)
Nitrogen-limited chemostat		6.9	6.1	(HENRY *et al.* 2010)
Glucose-limited chemostat		6.9	6.6	(HENRY *et al.* 2010)
Nitrogen-limited chemostat		6.9	6.6	(HENRY *et al.* 2010)
Glucose-limited chemostat		7	4.6	(CARTER AND JAGADISH 1978)
MM3+Citrate	16.9	7.3	3.6	(TYSON *et al.* 1979)
MM+Ethanol+Ammonia		7.5	4.7	(CARTER AND JAGADISH 1978)
EMM+Acetate+Pthalate	18.9	7.6	4.2	(TYSON *et al.* 1979)
MM+Dextrose+Threonine		7.6	4.6	(JOHNSTON *et al.* 1980)
MM+Dextrose+Ammonia+CHX		8.2	6.5	(HARTWELL AND UNGER 1977)

MM+Ethanol+Ammonia		8.3	5.9	(JAGADISH AND CARTER 1977)
MM+Acetate		8.5	6.1	(JAGADISH AND CARTER 1977)
Glucose-limited chemostat		8.6	6.5	(CARTER AND JAGADISH 1978)
Glucose-limited chemostat		9.1	5.9	(JAGADISH AND CARTER 1977)
Glucose-limited chemostat		11.7	8.4	(CARTER AND JAGADISH 1978)
MM+Dextrose+Ammonia+CHX		11.9	10.6	(HARTWELL AND UNGER 1977)
Glucose-limited chemostat	42.5	13.9	11.3	(BRAUER *et al.* 2008)
Leucine-limited chemostat	43.3	13.9	11.5	(BRAUER *et al.* 2008)
Phosphorous-limited chemostat	40.4	13.9	11.7	(BRAUER *et al.* 2008)
Sulfur-limited chemostat	31.3	13.9	11.9	(BRAUER *et al.* 2008)
Nitrogen-limited chemostat	32.8	13.9	12	(BRAUER *et al.* 2008)
Uracil-limited chemostat	47.8	13.9	12	(BRAUER *et al.* 2008)
Glucose-limited chemostat		17.9	12.5	(CARTER AND JAGADISH 1978)
Glucose-limited chemostat	34.3	21.6	15.6	(JAGADISH AND CARTER 1977)

589

590 **Table S2. Human cell cycle kinetics**

Cell type	T_d (h)	T_{G1} (h)	Reference
acute myeloblastic leukemia cells	49	24	(BASERGA 1985)
amnion cells	18.2	7.3	(SISKEN AND KINOSITA 1961)
amnion cells	19.5	9.5	(BASERGA 1985)
amnion cells	21.4	10.3	(SISKEN AND KINOSITA 1961)
ascites carcinoma cells	113	50	(BASERGA 1985)
basal cell carcinoma cells	67	36	(BASERGA 1985)
bone marrow cells	18	2	(BASERGA 1985)
BR:BT-549; NCI60 panel	53.9	30.9	(SCHERF *et al.* 2000; GARNER AND EASTMAN 2011), and this study
BR:HS 578T; NCI60 panel	53.8	30.5	(SCHERF *et al.* 2000; GARNER AND EASTMAN 2011), and this study
BR:MCF7; NCI60 panel	25.4	14.7	(SCHERF *et al.* 2000; GARNER AND EASTMAN 2011), and this study
BR:MDA-MB-231; NCI60 panel	41.9	23.7	(SCHERF *et al.* 2000; GARNER AND EASTMAN 2011), and this study
BR:T-47D; NCI60 panel	45.5	30.2	(SCHERF *et al.* 2000; GARNER AND EASTMAN 2011), and this study
CNS:SF-268; NCI60 panel	33.1	17.2	(SCHERF *et al.* 2000; GARNER AND EASTMAN 2011), and this study
CNS:SF-295; NCI60 panel	29.5	17.9	(SCHERF *et al.* 2000; GARNER AND EASTMAN 2011), and this study
CNS:SF-539; NCI60 panel	35.4	23.59	(SCHERF *et al.* 2000; GARNER AND EASTMAN 2011), and this study
CNS:SNB-19; NCI60 panel	34.6	21.3	(SCHERF *et al.* 2000; GARNER AND EASTMAN 2011), and this study
CNS:SNB-75; NCI60 panel	62.8	40.1	(SCHERF *et al.* 2000; GARNER AND EASTMAN 2011), and this study
CNS:U251; NCI60 panel	23.8	9.8	(SCHERF *et al.* 2000; GARNER AND EASTMAN 2011), and this study
CO:COLO 205; NCI60 panel	23.8	14.9	(SCHERF *et al.* 2000; GARNER AND EASTMAN 2011), and this study
CO:HCC-2998; NCI60 panel	31.5	19.2	(SCHERF *et al.* 2000; GARNER AND EASTMAN 2011), and this study
CO:HCT-116; NCI60 panel	17.4	8.5	(SCHERF *et al.* 2000; GARNER AND EASTMAN 2011), and this study
CO:HCT-15; NCI60 panel	20.6	10.9	(SCHERF *et al.* 2000; GARNER AND EASTMAN 2011), and this study
CO:HT29; NCI60 panel	19.5	13	(SCHERF *et al.* 2000; GARNER AND EASTMAN 2011), and this study
CO:KM12; NCI60 panel	23.7	11.4	(SCHERF *et al.* 2000; GARNER AND EASTMAN 2011), and this study
CO:SW-620; NCI60 panel	20.4	13.1	(SCHERF *et al.* 2000; GARNER AND EASTMAN 2011), and this study

colon epithelial cells	25	9	(BASERGA 1985)
epidermoid carcinoma cells	24	9	(BASERGA 1985)
Fibroblasts	18	5.5	(DEFENDI AND MANSON 1963)
HeLa	16.2	7.6	(KUMEI *et al.* 1989)
HeLa	19	12.1	(LUCIANI *et al.* 2001)
HeLa	19.4	11	(HAHN *et al.* 2009)
HeLa	20.4	14.9	(LUCIANI *et al.* 2001)
HeLa	21	8	(BASERGA 1985)
HeLa	25	13	(LENNARTZ AND MAURER 1964)
HeLa	26.6	19.7	(LUCIANI *et al.* 2001)
HeLa	27.6	21.8	(LUCIANI *et al.* 2001)
HeLa	28	13.5	(DEFENDI AND MANSON 1963)
HeLa	28	14	(LENNARTZ AND MAURER 1964)
high grade non-Hodgkins lymphoma cells	57	36	(BRONS *et al.* 1992)
Hodgkins lymphoma cells	62	37	(BRONS *et al.* 1992)
intermediate grade non-Hodgkins lymphoma cells	69	47	(BRONS *et al.* 1992)
KB	31.5	6.5	(BASERGA 1985)
Ki-67 reactive hyperplasia lymphoma cells	22	14	(BRONS *et al.* 1992)
LC:A549/ATCC; NCI60 panel	22.9	13.8	(SCHERF *et al.* 2000; GARNER AND EASTMAN 2011), and this study
LC:EKVX; NCI60 panel	43.6	29.2	(SCHERF *et al.* 2000; GARNER AND EASTMAN 2011), and this study
LC:HOP-92; NCI60 panel	79.5	46. 2	(SCHERF *et al.* 2000; GARNER AND EASTMAN 2011), and this study
LC:NCI-H226; NCI60 panel	61	41.2	(SCHERF *et al.* 2000; GARNER AND EASTMAN 2011), and this study
LC:NCI-H23; NCI60 panel	33.4	15.4	(SCHERF *et al.* 2000; GARNER AND EASTMAN 2011), and this study
LC:NCI-H322M; NCI60 panel	35.3	22.8	(SCHERF *et al.* 2000; GARNER AND EASTMAN 2011), and this study
LC:NCI-H460; NCI60 panel	17.8	12.6	(SCHERF *et al.* 2000; GARNER AND EASTMAN 2011), and this study
LC:NCI-H522; NCI60 panel	38.2	25.3	(SCHERF *et al.* 2000; GARNER AND EASTMAN 2011), and this study
LE:CCRF-CEM; NCI60 panel	26.7	12.1	(SCHERF *et al.* 2000; GARNER AND EASTMAN 2011), and this study
LE:HL-60(TB) ; NCI60 panel	28.6	16.2	(SCHERF *et al.* 2000; GARNER AND EASTMAN 2011), and this study
LE:K-562; NCI60 panel	19.6	10.1	(SCHERF *et al.* 2000; GARNER AND EASTMAN 2011), and this study
LE:MOLT-4; NCI60 panel	27.9	15.9	(SCHERF *et al.* 2000; GARNER AND EASTMAN 2011), and this study
LE:RPMI-8226; NCI60 panel	33.5	12.4	(SCHERF *et al.* 2000; GARNER AND EASTMAN 2011), and this study

LE:SR; NCI60 panel	28.7	14.0	(SCHERF *et al.* 2000; GARNER AND EASTMAN 2011), and this study
low grade non-Hodgkins lymphoma cells	107	80	(BRONS *et al.* 1992)
Lymphocytes	30.4	14.2	(AOKI AND MOORE 1970)
Lymphocytes	33.1	15.1	(AOKI AND MOORE 1970)
Lymphocytes	38.4	21.2	(AOKI AND MOORE 1970)
Lymphocytes	43.5	25.9	(AOKI AND MOORE 1970)
Lymphocytes	72.5	49.4	(AOKI AND MOORE 1970)
Lymphocytes	76.5	55	(AOKI AND MOORE 1970)
MCF-7 breast cancer cells	24	14.4	(BRUNNER *et al.* 1989)
ME:LOX IMVI; NCI60 panel	20.5	11.2	(SCHERF *et al.* 2000; GARNER AND EASTMAN 2011), and this study
ME:M14; NCI60 panel	26.3	15.9	(SCHERF *et al.* 2000; GARNER AND EASTMAN 2011), and this study
ME:MALME-3M; NCI60 panel	46.2	30.2	(SCHERF *et al.* 2000; GARNER AND EASTMAN 2011), and this study
ME:MDA-MB-435; NCI60 panel	25.8	10.1	(SCHERF *et al.* 2000; GARNER AND EASTMAN 2011), and this study
ME:SK-MEL-2; NCI60 panel	45.5	25	(SCHERF *et al.* 2000; GARNER AND EASTMAN 2011), and this study
ME:SK-MEL-28; NCI60 panel	35.1	24.9	(SCHERF *et al.* 2000; GARNER AND EASTMAN 2011), and this study
ME:SK-MEL-5; NCI60 panel	25.2	17.7	(SCHERF *et al.* 2000; GARNER AND EASTMAN 2011), and this study
ME:UACC-257; NCI60 panel	38.5	28.3	(SCHERF *et al.* 2000; GARNER AND EASTMAN 2011), and this study
ME:UACC-62; NCI60 panel	31.3	21.2	(SCHERF *et al.* 2000; GARNER AND EASTMAN 2011), and this study
melanoma cells	46	20	(BASERGA 1985)
NCI-H292	18.5	6.8	(HAHN *et al.* 2009)
OV:IGROV1; NCI60 panel	31	21.6	(SCHERF *et al.* 2000; GARNER AND EASTMAN 2011), and this study
OV:NCI/ADR-RES; NCI60 panel	34	23.1	(SCHERF *et al.* 2000; GARNER AND EASTMAN 2011), and this study
OV:OVCAR-3; NCI60 panel	34.7	19.9	(SCHERF *et al.* 2000; GARNER AND EASTMAN 2011), and this study
OV:OVCAR-4; NCI60 panel	41.4	19.0	(SCHERF *et al.* 2000; GARNER AND EASTMAN 2011), and this study
OV:OVCAR-5; NCI60 panel	48.8	28.5	(SCHERF *et al.* 2000; GARNER AND EASTMAN 2011), and this study
OV:OVCAR-8; NCI60 panel	26.1	13.3	(SCHERF *et al.* 2000; GARNER AND EASTMAN 2011), and this study
OV:SK-OV-3; NCI60 panel	48.7	39.9	(SCHERF *et al.* 2000; GARNER AND EASTMAN 2011), and this study
PR:DU-145; NCI60 panel	32.3	18.2	(SCHERF *et al.* 2000; GARNER AND EASTMAN 2011), and this study

PR:PC-3; NCI60 panel	27.1	15.4	(SCHERF *et al.* 2000; GARNER AND EASTMAN 2011), and this study
RE:786-0; NCI60 panel	22.4	13.5	(SCHERF *et al.* 2000; GARNER AND EASTMAN 2011), and this study
RE:A498; NCI60 panel	66.8	41.1	(SCHERF *et al.* 2000; GARNER AND EASTMAN 2011), and this study
RE:ACHN; NCI60 panel	27.5	14.9	(SCHERF *et al.* 2000; GARNER AND EASTMAN 2011), and this study
RE:CAKI-1; NCI60 panel	39	25.0	(SCHERF *et al.* 2000; GARNER AND EASTMAN 2011), and this study
RE:RXF 393; NCI60 panel	62.9	31.1	(SCHERF *et al.* 2000; GARNER AND EASTMAN 2011), and this study
RE:SN12C; NCI60 panel	29.5	15.5	(SCHERF *et al.* 2000; GARNER AND EASTMAN 2011), and this study
RE:TK-10; NCI60 panel	51.3	29.4	(SCHERF *et al.* 2000; GARNER AND EASTMAN 2011), and this study
RE:UO-31; NCI60 panel	41.7	26.5	(SCHERF *et al.* 2000; GARNER AND EASTMAN 2011), and this study
rectum epithelial cells	48	33	(BASERGA 1985)
stomach epithelial cells	24	9	(BASERGA 1985)
H. sapiens diploid fibroblasts	18	6.6	(BASERGA 1985)

591

592 An additional file (**Supplementary File 1**) is attached and contains all raw immunoblot images generated

593 and used in this study.

594

FIGURE 1

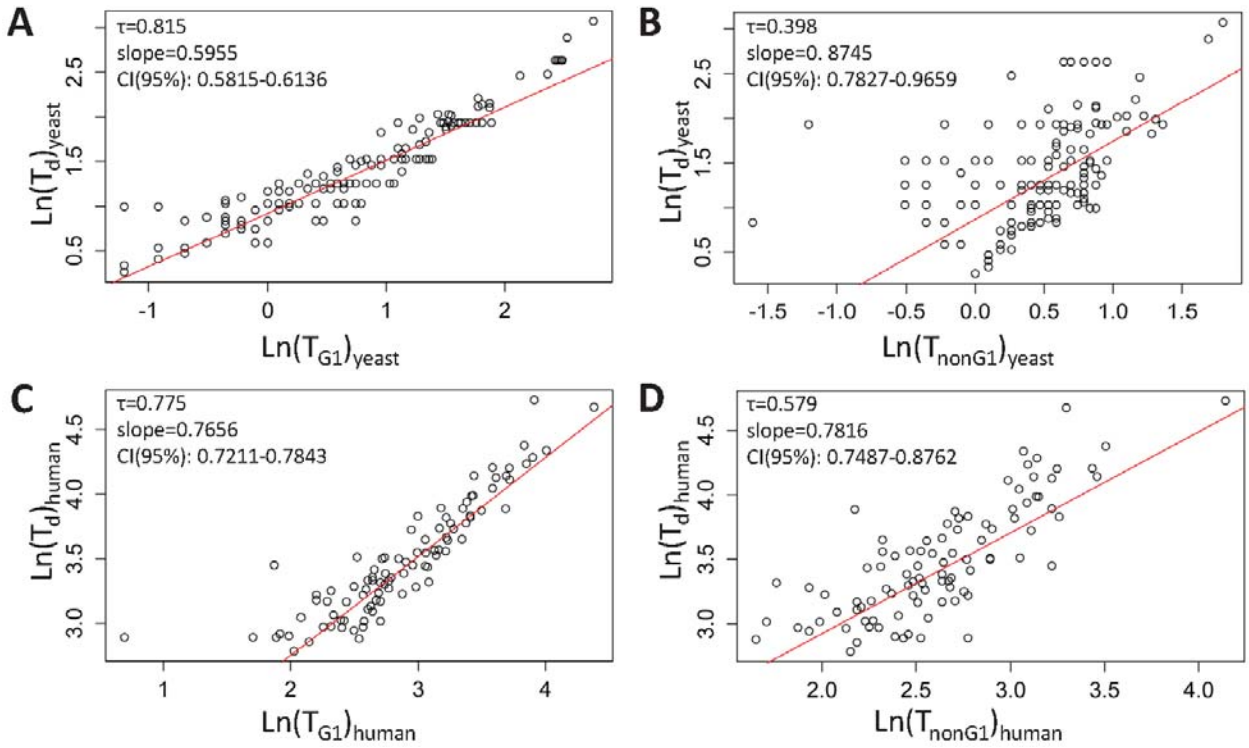
A
τ=0.815
slope=0.5955
CI(95%): 0.5815-0.6136
Ln(Td)yeast
Ln(TG1)yeast
B
τ=0.398
slope=0. 8745
CI(95%): 0.7827-0.9659
Ln(Td)yeast
Ln(TnonG1)yeast
C
τ=0.775
slope=0.7656
CI(95%): 0.7211-0.7843
Ln(Td)human
Ln(TG1)human
D
τ=0.579
slope=0.7816
CI(95%): 0.7487-0.8762
Ln(Td)human
Ln(TnonG1)human

FIGURE 2

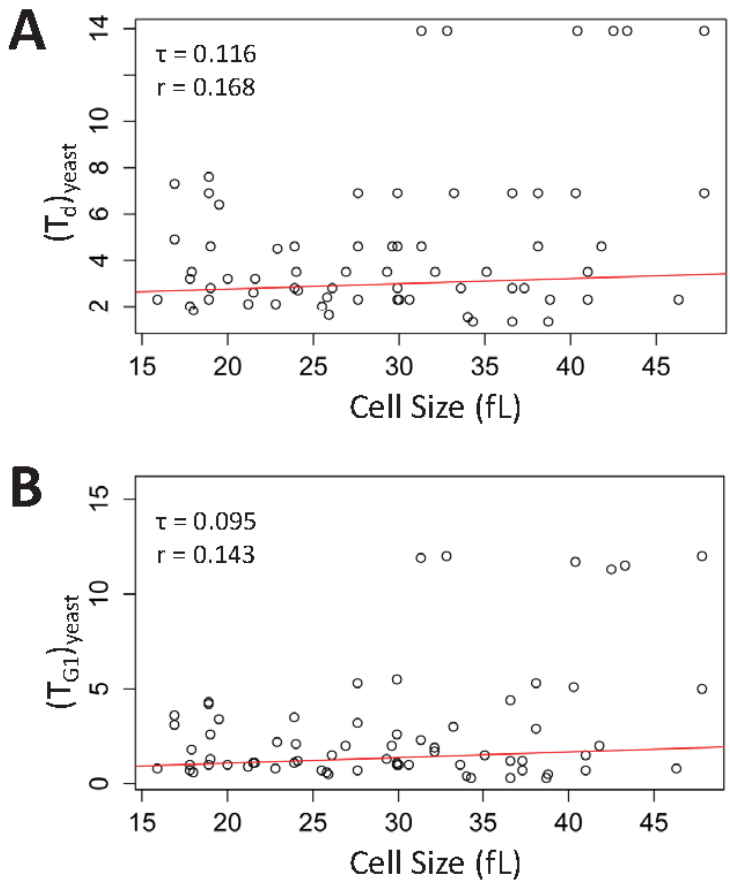
A
τ = 0.116
r = 0.168
$(T_d)_{yeast}$
Cell Size (fL)
B
τ = 0.095
r = 0.143
$(T_{G1})_{yeast}$
Cell Size (fL)

600 FIGURE 3

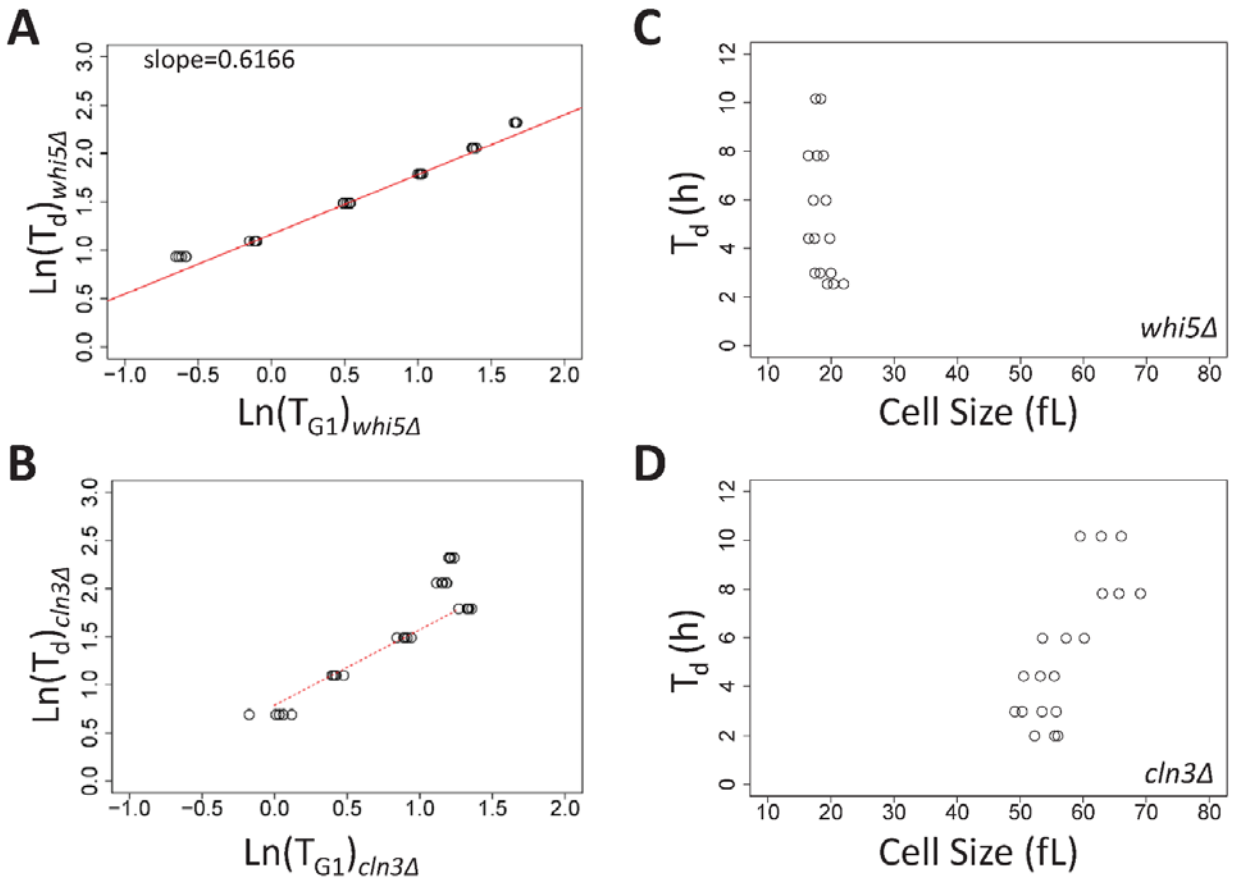

601

602

603 FIGURE 4

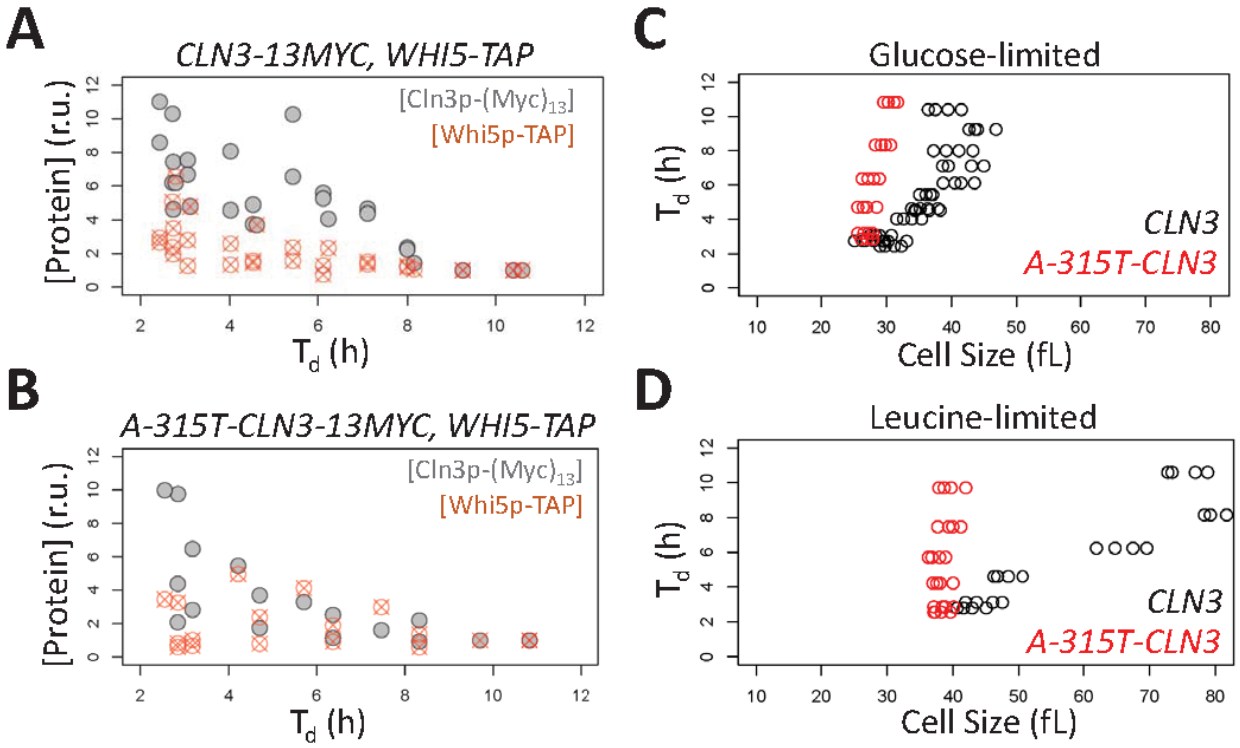

604

605 FIGURE S1

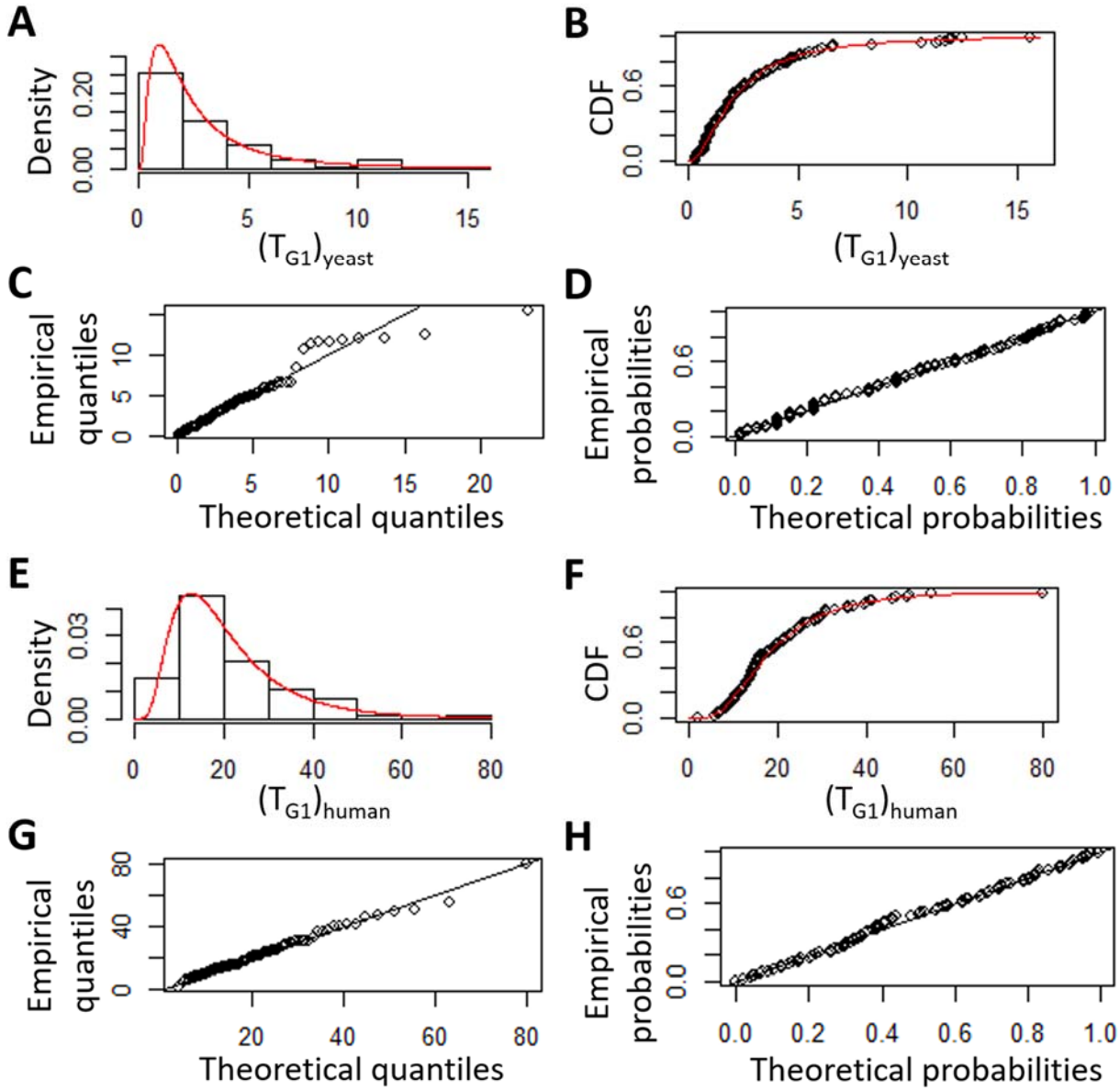

606

FIGURE S2

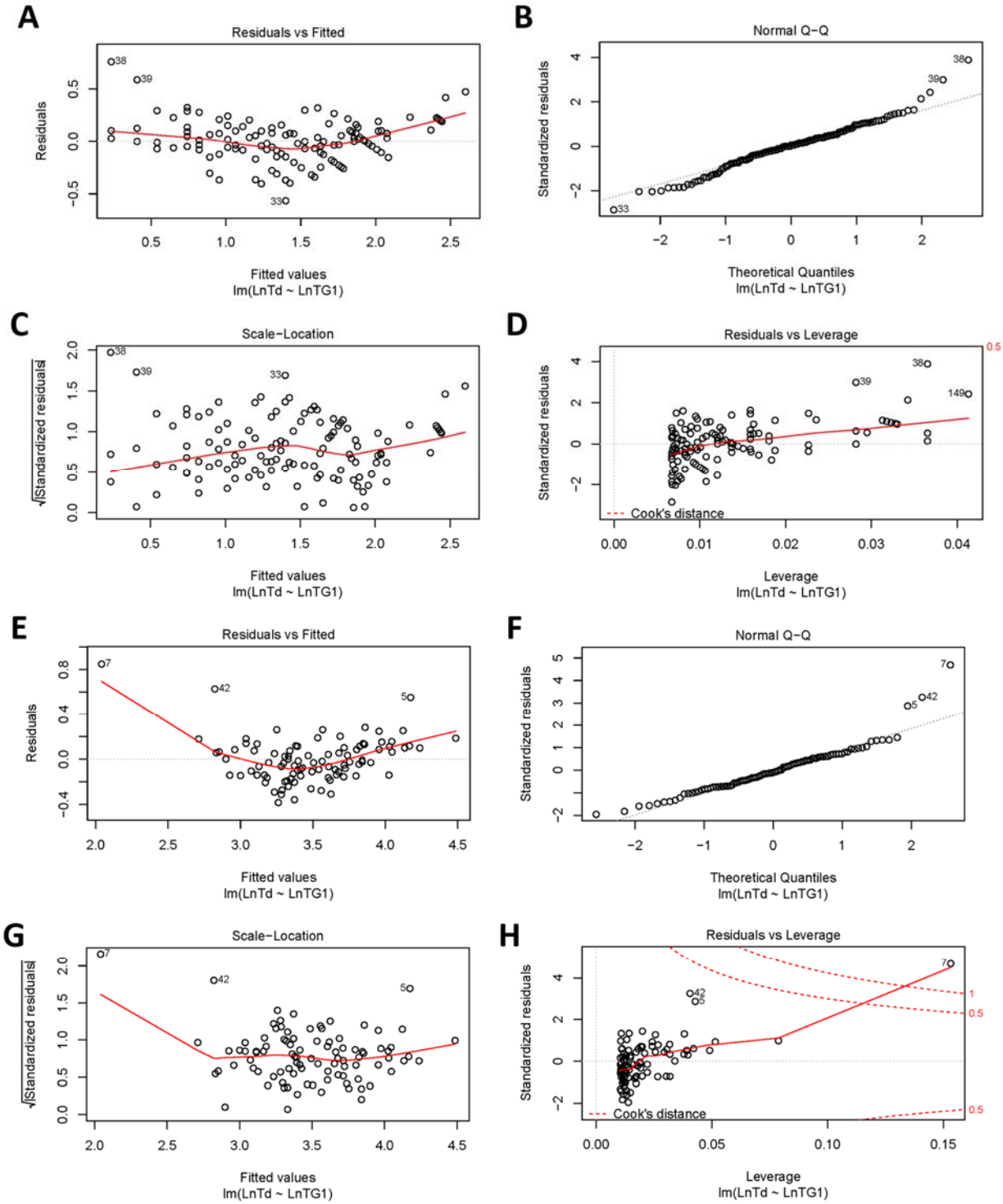
A
Residuals vs Fitted
Residuals
Fitted values
lm(LnTd ~ LnTG1)
B
Normal Q−Q
Standardized residuals
Theoretical Quantiles
lm(LnTd ~ LnTG1)
C
Scale−Location
√|Standardized residuals|
Fitted values
lm(LnTd ~ LnTG1)
D
Residuals vs Leverage
Standardized residuals
Cook's distance
Leverage
lm(LnTd ~ LnTG1)
E
Residuals vs Fitted
Residuals
Fitted values
lm(LnTd ~ LnTG1)
F
Normal Q−Q
Standardized residuals
Theoretical Quantiles
lm(LnTd ~ LnTG1)
G
Scale−Location
√|Standardized residuals|
Fitted values
lm(LnTd ~ LnTG1)
H
Residuals vs Leverage
Standardized residuals
Cook's distance
Leverage
lm(LnTd ~ LnTG1)

Western blot controls for detection of Cln3p-13Myc and Whi5p-TAP.

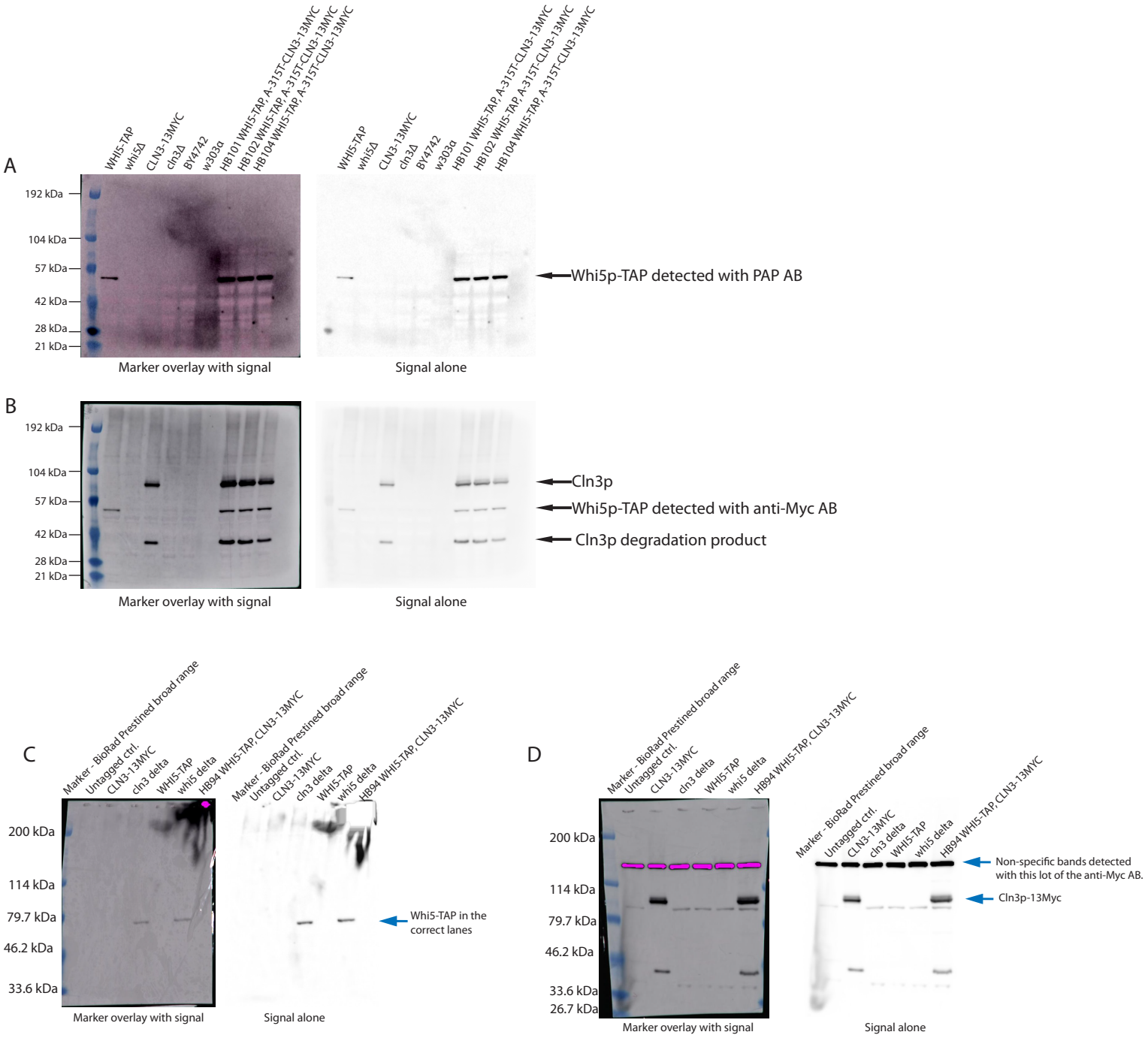

A. Western blot of proteins extracted from the strains indicated. The blot was first probed with the PAB antibody to show the detection of Whi5p-TAP in the appropriate lanes at the right size. B. Same blot as in A but probed additionally with the anti-Myc antibody followed by anti-rabbit HRP antibody for detection. This method allowed us to detect both Cln3p-13Myc and Whi5p-TAP on the same blot using the same exposure. C and D. Additional earlier control western blot performed with an earlier lot of the anti-Myc antibody. C. Detection of Whi5p-TAP probed with the PAP antibody. D. Different blot of the same samples run in C, probed with the anti-Myc antibody. Note the presence of dark non-specific bands detected with this lot of the anti-Myc antibody.

Western blots for quantification of Cln3p and Whi5p at different doubling times (T_D) from chemostat experiments.

Suppl. File 1
Page-2

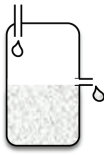

Cell samples collected and frozen at the indicated doubling times, controlled by media in/out flow rate.

Proteins extracted and run on gel in duplicate, followed by transfer to a membrane and staining with Ponceau S (column 1).

Blot probed first with PAP antibody (not shown) and then with anti-Myc antibody and anti-Rabbit HRP secondary antibody for detection and quantification of Whi5p-TAP and Cln3p-$(Myc)_{13}$ (columns 3 and 4).

Column 1	Column 2	Column 3	Column 4
Ponceau S (total protein)	Marker overlay (for size only)	Raw signal	Signal (cropped with background subtract for quantification)

Glucose limiting, Chemostat 1, Set 1 (Strain HB94)

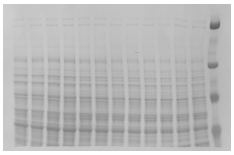

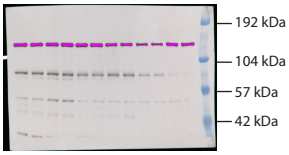

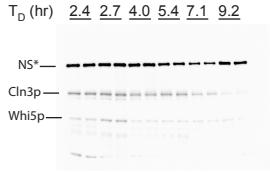

* indicates a non-specific band that was detected with an earlier lot of the anti-MYC antibody.

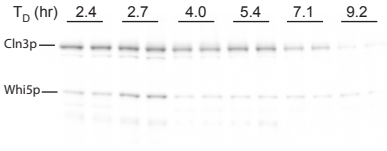

Glucose limiting, Chemostat 1, Set 2 (Strain HB94)

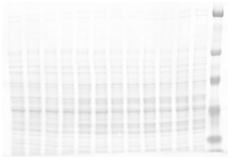

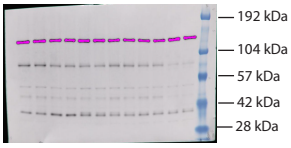

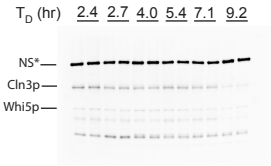

* indicates a non-specific band that was detected with an earlier lot of the anti-MYC antibody.

Glucose limiting, Chemostat 2, Set 1 (Strain HB97)

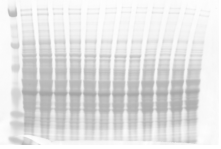

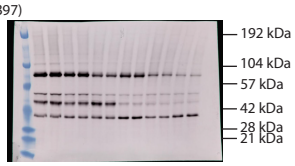

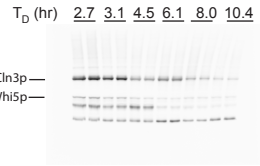

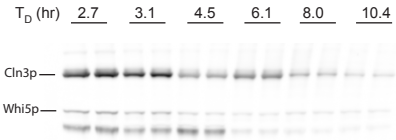

Glucose limiting, Chemostat 2, Set 2 (Strain HB97)

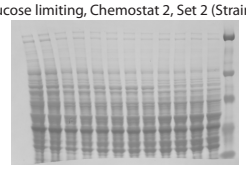

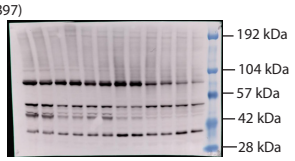

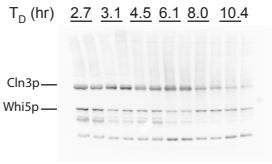

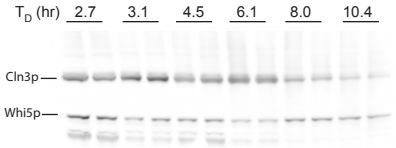

Leucine limiting (Strain HB97)

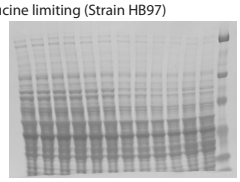

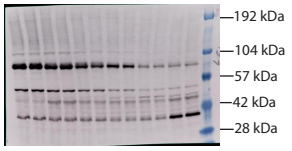

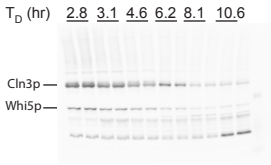

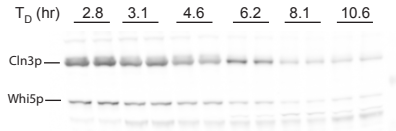

Glucose limiting (Strain HB104-A315T) set1 wb2

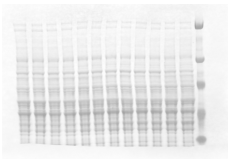

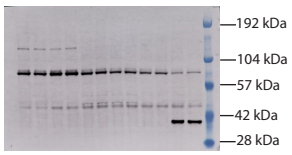

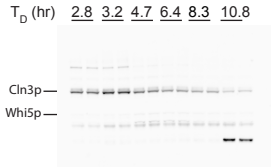

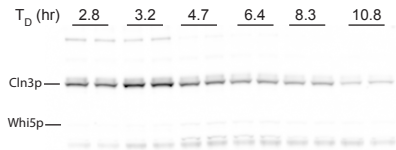

Glucose limiting (Strain HB104-A315T set2 wb1

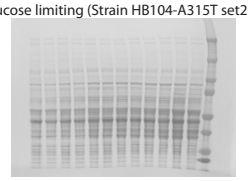

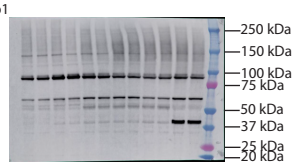

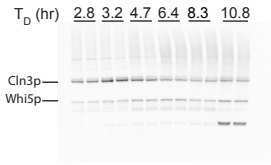

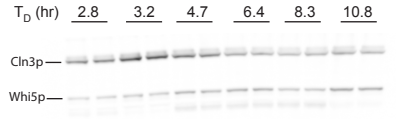
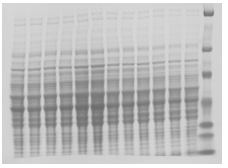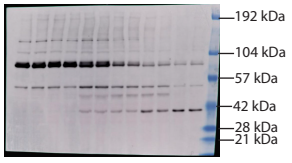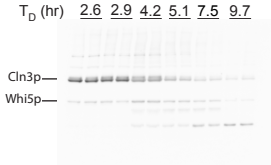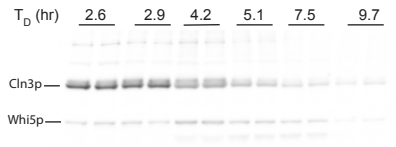
Leucine limiting (Strain HB104-A315T set1 wb1